Part I: THEORETICAL BACKGROUND

NON-ERGODIC PROBABILISTIC SEISMIC HAZARD METHODOLOGY USING PHYSICS-BASED GROUND MOTION PREDICTION: THE CASE OF L'AQUILA, ITALY

JEDIDIAH JOEL AGUIRRE[1,2],
BRUNO RUBINO[1], MAURIZIO VASSALLO[3],
GIUSEPPE DI GIULIO[3]
AND FRANCESCO VISINI[4]

[1] *Università Degli Studi Dell'Aquila*

67100 L'Aquila, Italy

[2] *University of the Philippines*

4031 Los Baños, Laguna, Philippines

[3] *Istituto Nazionale di Geofisica e Vulcanologia – Sezione dell'Aquila*

67100 L'Aquila, Italy

[4] *Istituto Nazionale di Geofisica e Vulcanologia – Sezione di Pisa*

56125 Pisa, Italy

(received: 4 January 2020; revised: 9 February 2020;
accepted: 15 March 2020; published online: 1 April 2020)

Abstract: A non-ergodic probabilistic seismic hazard analysis (PSHA) utilizing the physics-based ground motion prediction was proposed in this study to minimize the increasing uncertainties in the use of empirical equations. The City of L'Aquila in Italy was used for illustrative purposes due to the availability of data and the historical seismicity of the site. A total of 28 seismic sources were identified in this study located within a 100 km radius from the city. Fault properties such as geometry and location were obtained from the literature, while the fault occurrence rates were obtained using the FiSH Code. A modified time-weakening friction law was proposed to model the seismic energy released by an earthquake. Uncertainties in different rupture scenarios were characterized through the Guttenberg-Richter Relations and the Characteristic Brownian Time Passage. Uncertainties in distances were characterized through probability mass functions, which were used to calculate the ground motion exceedance probabilities. The 1D elastodynamic equation coupled with the Hooke's law was used to predict the peak ground acceleration (PGA), a measure of the ground shaking level. A hazard curve, which is a plot of PGA and its

recurrence, was constructed and compared with the results of the study of Valentini, *et al.*, *AGU 100: Advancing Earth and Space Science* (2019). The method proposed in this study predicts a higher hazard rates for PGAs less than 0.70 g, which implies that the ground motion was overestimated for very far sources. In contrast, lower hazard curves were observed for PGAs greater than 0.70g which can be attributed to fewer seismic sources considered in this study.

Keywords: non-ergodic probabilistic seismic hazard analysis, physics-based ground motion prediction, modified time-weakening friction law, peak ground acceleration, hazard curve, City of L'Aquila

DOI: https://doi.org/10.34808/tq2020/24.2/a_part1

1. Introduction

Upon the failure of rocks in a causative fault, an earthquake is produced due to the sudden release of energy built on the Earth's crust through seismic waves [1, 2]. As a result, severe earthquakes worldwide have claimed thousands of lives and billions of euros in damages.

On April 6^{th}, 2009 the City of L'Aquila was devastated by an M_w 6.3 earthquake claiming 300 deaths, around 1500 injured, and approximately € 25 billion in damages [3]. The hypocentral depth is about 8.8 to 9 km with a normal style of faulting with a dip of around 43 degrees. The population nearby the epicenter is around 100,000 making the city very seismically vulnerable [3, 4]. This earthquake is deemed to have had the highest death toll and the highest economic loss in the EU. Figure 1 shows the rubbles of some structures in L'Aquila that collapsed during the earthquake in April 2009.

Earthquakes do not kill, but it is the *secondary or seismic hazards* that they trigger [5, 1]. According to Kramer [1], these hazards include ground shaking, structural hazards, liquefaction, landslides, retaining structural failures, lifeline hazards, tsunamis and seiches. For the purpose of discussion, this study will be focused on the ground shaking hazard only, while the other above mentioned seismic hazards will not be covered by it the scope.

The occurrence of earthquakes cannot be fully predicted as to when and where they can occur, but the secondary hazards can be mitigated through proper coordination of seismologists, engineers, social scientists, and policy-making bodies in an area. Hence, there is a need to estimate the underlying *seismic hazard* in terms of ground shaking levels on site required for engineers to be considered in their design and retrofit structures which can collapse during an earthquake.

1.1. Seismic Hazard Analysis

The Seismic Hazard Analysis (SHA) is a method of estimating the feasible ground shaking levels on a site [1]. At the present time, there are two existing ways of estimating ground shaking levels: either deterministic or probabilistic. The *Deterministic Seismic Hazard Analysis* (DSHA) aims to determine exactly the maximum controlling earthquake coming from a certain seismic source that can affect the site on a worst-case scenario basis. On the other hand, the *Probabilistic Seismic Hazard Analysis* (PSHA) is a methodology that estimates the ground

Figure 1. Structural Damage during the Mw 6.3 Abruzzo Earthquake in 2009
Source: https://www.britannica.com/event/LAquila-earthquake-of-2009

shaking hazard in a given place assuming the chances of exceeding a certain level of ground shaking that occurred in the past within a specified period interval of validity.

To further understand these two methods, the outcomes offered by these methods should be considered:

Deterministic

"The peak ground acceleration (PGA) on the site is 0.65g resulting from an earthquake of a magnitude of 6.3 on the Paganica Fault at a distance of 12km from the site"

Probabilistic

"The PGA on the site is 0.45 g with a 10% probability of being exceeded in a 50-year period"

Both these methods use the same information such as past earthquakes, fault geometries, geology, etc. to be discussed later in this paper, however, the PSHA incorporates uncertainties in such data since the occurrence of an earthquake is random by nature. The PSHA can be viewed as a series of deterministic approaches with consideration of uncertainties. The expected output in the PSHA is a *hazard curve*, which describes the hazard level with respect to the ground shaking level on a site [1].

1.1.1. Deterministic Approach

Kramer [1] summarized the DSHA into four steps as shown in Figure 2.

Step 1. In DSHA, all types of seismic sources within a certain distance which can greatly affect a site must be considered. These include point sources (such as

volcanoes), fault lines, or fault planes. These kinds of sources will be discussed in a later part of this paper.

Step 2. The shortest distance from the seismic source to the site, also known as the *source-to-site distance*, is calculated.

Step 3. Using some ground motion prediction equations (GMPE) which relate the distance and magnitude of the earthquake to a ground motion parameter, say the PGA, the existing seismic hazard can be determined "exactly". Hence, the controlling earthquake that will produce the strongest shaking effect will be selected.

Step 4. Lastly, the values of different ground shaking parameters are reported for the site with the corresponding source-to-site distance and magnitude of the earthquake.

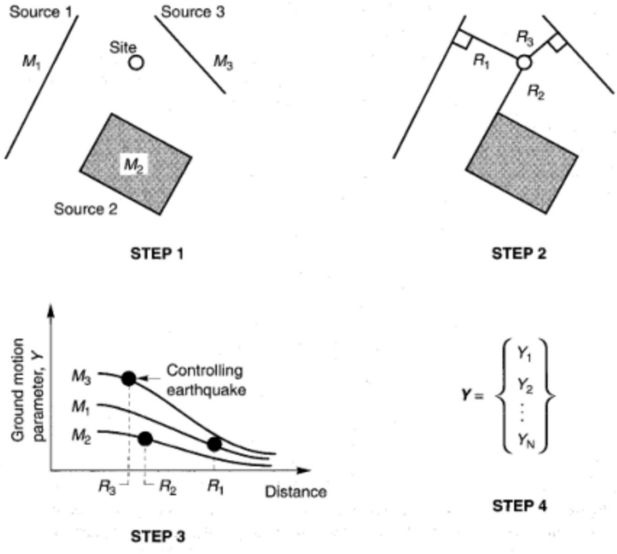

Figure 2. Steps in DSHA
Source: Kramer, 1996 [1]

Based on this framework, the contributor of the overall seismic hazard on a site will be one controlling earthquake only. It is worth noting that other data such as fault geometries, paleoseismology, site properties (the type of soil on the site) are also needed to fully describe the seismic hazard on a site [1, 5].

The problem with the deterministic approach is that the information keeps changing from time to time, hence, it is not proper to say that the seismic hazard is "determined" exactly, but what happens is that the seismic hazard changes from time to time.

1.1.2. **Probabilistic Approach**

The PSHA will be discussed later in a separate Section. A glimpse of the PSHA is shown here for illustrative purposes and to compare it with the deterministic approach.

Hutchings and Viegas [6] summarized the PSHA dividing it into four steps as shown in Figure 3.

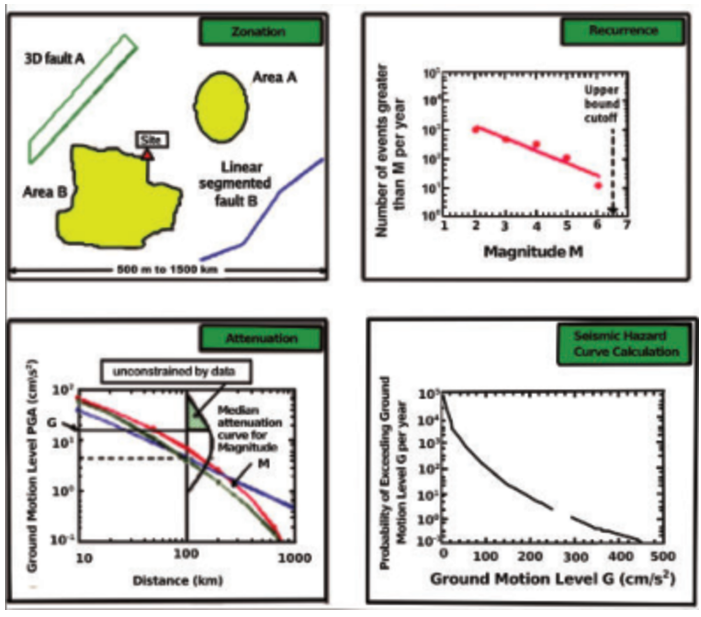

Figure 3. Steps in PSHA
Source: Hutchings and Viegas, 2012 [6]

Step 1 (Zonation). Similarly to the DSHA, all seismic sources that are found at a certain distance which may contribute to the seismic hazard are considered. However, the uncertainties in the source-to-site distances for all seismic sources are formulated through the *probability density functions (PDF).*

Step 2 (Recurrence). Earthquake occurrence in all sources is modeled by a recurrence law. The frequency of earthquakes as a function of the earthquake size (or magnitude) is established, and the recurrence parameters are calculated to be used later in hazard calculations.

Step 3 (Attenuation). GMPEs are used just like in the DSHA, but with consideration given to uncertainties. Due to the development of the PSHA Methodology, the ground motion parameter can be predicted by the existing physical laws on rupture dynamics [7] with uncertainties being taken into account considering a sufficient number of the ground motion predictions [8].

Step 4 (Seismic Hazard Curve Calculation). A hazard rate is calculated in terms of the probability of exceedance or hazard rates, as a function of the ground motion parameter calculated in Step 3.

Based on the probabilistic approach, all kinds of possible earthquake occurrences coming from all possible seismic sources are incorporated into the seismic hazard on a site. As mentioned above, the PSHA is just a series of deterministic approaches with a defined probability of exceedance [9].

The PSHA has a concept of a *return period*, just like strong winds or flooding [10] which is good, as information keeps on changing from time to time. Therefore, it is much better to conduct a PSHA than a DSHA. Many engineers are shifting to the probabilistic approach and tend to abandon the deterministic approach.

1.1.3. Risk Engineering Decisions

The major difference between the two methods is based on what type of decisions the policy-making body must make [9]. Table 1 shows the how McGuire presents the approach to be taken by the engineer and risk mitigation agencies depending on the decision to be made. According to the building code, it is recommended that a structure must withstand a reference peak ground acceleration (PGA) which corresponds to a reference probability of exceedance of 10

Table 1. The predominant approach for several engineering decisions
Source: McGuire, 2001 [9]

DECISION	QUANTITATIVE ASPECTS OF DECISION	PREDOMINANT APPROACH
Seismic design	Highly quantitative	Probabilistic
Retrofit design	Highly quantitative	Probabilistic
Insurance/Reinsurance	Highly quantitative	Probabilistic
Design of redundant industrial systems	Quantitative or Qualitative	Both
Training and plans for emergency purposes	Mostly qualitative	Deterministic
Plans for post-earthquake recovery	Mostly qualitative	Deterministic
Plans for long-term recovery, local	Mostly qualitative	Deterministic
Plans for long-term recovery, regional	Mostly quantitative	Probabilistic

Both methods are applicable for the design of complex structures such as industrial power plants depending on the seismic environment of the site. If the site has many surrounding faults, then, it is desirable to choose the PSHA. If lifelines are to be installed on a site where an active fault is crossed, then the DSHA can be employed instead [9]. This is because the site itself is subjected to the fault

movement and a maximum credible earthquake must be determined to design the lifelines seismically.

Planning for recovery from earthquake losses, whether immediately or in a long term, is a very tedious process where multiple earthquake scenarios cannot be considered, hence, it will be more effective, if only a single scenario earthquake is to be considered for risk mitigation practices and emergency plans. However, for a regional long-term recovery, it is advisable to use the probabilistic approach considering many seismic sources that are present in an entire region, or a country [9].

1.2. Evolution of PSHA Methodology

According to McGuire [11], two different efforts, working independently, ushered a new era of a probabilistic approach whose works combined in 1966. Carl Allin Cornell from the Standford University produced his PhD Dissertation in 1964 entitled *Stochastic Processes in Civil Engineering*, ocused on factors affecting the engineering decisions through probability distributions. Then, Universidad Nacional Autonoma de Mexico (UNAM) conducted several studies on earthquake ground motions and their dependence on the magnitude and distance, and frequencies of ground motions and earthquake occurrences for the engineering design of structures, which were pioneered by the then PhD student Luis Esteva, Prof. Emilio Rosenblueth, and their colleagues.

On 1966, the "probabilistic seismic hazard" was derived from among the relationships of earthquake magnitudes and their respective occurrence rates, earthquake locations, and the resulting ground motions on the site. It was Cornell, who once taught at UNAM, who talked to Esteva and convinced him and his colleagues at UNAM to formalize the concept of the probabilistic approach.

1.2.1. **First Formulation**

Cornell [10] published a paper which became the first PSHA formulation. Assuming a Poisson process of the occurrence of earthquakes, he formulated the probability that zero earthquakes having a minimum Modified Mercalli Intensity (MMI) level would be exceeded for a certain time period considering a minimum magnitude of interest m_0:

$$F_{I_{max}}(i) = \exp\left[-\nu C G \exp\left(\frac{-\beta_i}{c_2}\right)\right], \quad i \geq i' \tag{1}$$

where $F_{I_{max}}$ is the probability of occurrence that an annual maximum intensity I_{max} will occur (usually for $t = 1$ year), ν is the rate of occurrence of a fault, C, G and c_2 are constants related to the ground motion parameters depending on the magnitude of the earthquake and the geometry of the fault, $\beta = b\ln 10$ with b being the Guttenburg-Richter (G-R) slope from the statistical regression of earthquakes, and i' is some lower limit of the MMI Intensity. In his paper, faults can be a point, a line, or a plane. He also pointed out that in the case


Figure 4. Pioneers of the PSHA Methodology. Cornell C. Allin (1938 – 2007), and Esteva Luis (1935 –).
Source: McGuire, 2007 [11]

of many seismic sources, the probability of exceedance was a sum of individual contributions of all faults.

1.2.2. Second Formulation

In 1970, the PSHA was generalized using the concept of the total probability theorem [11]:

$$P(Y>y) \approx \sum_{i=1}^{N} \nu_i \int\int P[Y>y|M,R]\, f(m,r) dm\, dr] \tag{2}$$

where Y and y are ground motion parameters, ν is the occurrence rate of each seismic source i, $P[Y>y|M,R]$ is the conditional probability that Y will exceed a certain value of y given a magnitude M and the *source-to-site* distance R, and $f(m,r)$ is the PDF of magnitude m and distance r. Future research regarding the formulation (2) is the treatment of uncertainties which is not included in (1) which is incorporated in the conditional probability. Usually, this probability takes after normal distribution, which assumes that the ground motion parameter Y is lognormally distributed, and the standard deviation in the Z-transform is composed of aleatory (due to the randomness of the ground motion) and epistemic (due to the lack of data and knowledge) uncertainties [12, 13]. Next, the contribution to the overall seismic hazard is not assessed until the *disaggregation* [14] or *deaggregation* is formulated by McGuire in 1995 [15].

1.2.3. Third Formulation

In 1985, (2) was reformulated by McGuire [15] by introducing uncertainties in the number of standard deviations used in the Ground Motion Prediction Equations (GMPEs):

$$\lambda(Y>y) = \sum_{i=1}^{N} = \nu_i \int\int P[Y>y|M,R,\varepsilon]\, f_M(m) f_R f_\varepsilon(\varepsilon) dm\, dr\, d\varepsilon \tag{3}$$

where $\lambda(Y > y)$ is the hazard rate corresponding to exceedance of the ground motion parameter y, $P[Y > y|M,R,\varepsilon]$ is the Heaviside step function:

$$P[Y > y|M,R,\varepsilon] = H[\ln Y(M,R,\varepsilon) - \ln y] \tag{4}$$

which is zero, if $\ln Y(M,R,\varepsilon)$ is less than $\ln y$ or a given magnitude-distance-standard deviation triple (M,R,ε), and one otherwise; $f_M(m)$ is the PDF of magnitude m, $f_R(r)$ is the PDF of the source-to-site distance, and $f_\varepsilon(\varepsilon)$ is the PDF of the number of standard deviations ε which is normally distributed. The difference in the PDF expressed in (2) assumes in (3) that $f(m,r)$ can be expressed as a product of PDFs of the magnitude and distance, and so the ground motion dependence on magnitude and distance is incorporated into GMPEs which are based on the regression of ground motions over a certain region [1, 14]:

$$\ln y = f(M,R,\theta) + \varepsilon\,\sigma_{\ln y} \tag{5}$$

where θ is the parameter related to the style of faulting or the kinematic of the fault source and/or soil type, and $\sigma_{\ln y}$ is the standard deviation of the natural logarithm of the ground motion parameter y.

1.2.4. **Non-Ergodic PSHA**

In 1999, Anderson and Brune [12] introduced the concept of the *Non-Ergodic PSHA*, which abandons the ergodic assumption of PSHA in the use of GMPEs. The ergodic assumption implies that the ground motion parameters in space are treated in the PSHA as the uncertainty over time at a single point. Regions without a strong ground motion database use GMPEs developed for some other regions, and some engineers tend to abuse them without knowing their applicability in those regions. Hence, uncertainties tend to mount, thus affecting the seismic hazard level. They mentioned that the ergodic assumption tended to overestimate the ground motion parameter Y due to increased uncertainties in the standard deviation in (5) especially for longer return periods of earthquakes.

In their paper, Anderson and Brune [12] have mentioned that the ergodic assumption means that the aleatory uncertainty is present in the PSHA, particularly in the GMPEs. Hence, the objective of their study is to eliminate or minimize the aleatory uncertainties in the analysis, and epistemic uncertainties will remain. The seismic hazard will not be overestimated with the availability of more data and knowledge about the earthquake processes in a certain site.

Landwehr et al. [13] made a non-ergodic GMPE, through a Varying Coefficients Model (VCM) applicable in California. They allowed the coefficients of the GMPE to vary spatially to incorporate effects of source, site, and path variations in the equation. Thus, the epistemic uncertainties are suppressed per site, while the aleatory uncertainty is modeled for the whole of California. As a result, the GMPE produces a reduction of 40% in the aleatory uncertainty which can significantly affect the seismic hazard. Also, it was observed that the epistemic uncertainty was smaller on sites where events or stations were close, and large where there was little data.

Another work on the Non-Ergodic perspective is the study of Kotha, Bindi and Cotton [16] which improved the GMPEs in Europe and in the Middle East towards a Non-Ergodic PSHA. Using the strong ground motion data sets from the Reference Database for the Seismic Ground-Motion in Europe (RESOURCE), they established region-specific for Europe and Middle East, and site-specific GMPEs for Italy and Turkey. The results of their shift from the ergodic to non-ergodic PSHA reveal a change of 25% in the hazard values in region-specific, while larger changes as much as 50% in site-specific GMPEs.

It is shown in these works that the seismic hazard can be lowered significantly with the improvement in the ground motion prediction schemes by minimizing the aleatory uncertainty. Also, if there is an advance in knowledge of faulting and the available data, the epistemic uncertainties can be eliminated [12, 15].

1.2.5. Non-Ergodic PSHA by Physics-Based Ground Motion Prediction

While some researchers such as Landwehr et al. [13] tried to minimize the aleatory uncertainties in the GMPE, others tried to use a physical model rather than a regression model since more data is available to explain the physics behind earthquake occurrences from the failure of rocks in a seismic source. The Southern California Earthquake Center (SCEC) recommended that a physics-based approach of the ground motion prediction was more suitable in minimizing the aleatory uncertainties than using regression-based GMPEs, since the earthquake occurrence was far more complex than what statistics could offer, which was later endorsed by the National Research Council on 2003 in the US, as mentioned by Hutchings and Viegas [6].

The rupture of faults and ground displacements are governed by the Elastodynamic Equation with the proper equations related to material properties of the fault such as the Hooke's Law [17]. Such a model will be thoroughly discussed in Section 2 of this paper.

This approach started when Hutchings et al [18] used the deterministic approach of solving the 3D elastodynamic equation with rupture dynamics using empirical Green Functions, which is a representation function of the ground displacement. Computing all the scenarios for all faults in an area, and with their corresponding earthquake recurrence properties, hazard rates can be assessed in the same way as before as given in (2). In this approach, the probability term is obtained by creating a library of synthetic ground motions by employing uncertainties in fault parameters such as Asperities (strongest fault zone), Rise Time, Rupture Roughness, Rupture Velocity, Healing Velocity, Stress Drop, Hypocenter depth, and Energy released during an earthquake, allowing them to simulate different rupture scenarios for earthquakes.

Hutchings and Viegas [6] suggested a new way of conducting the PSHA, which was also employed in the work of Hutchings et al. [18] in the simulation of the 1999 Athens Earthquake with a moment magnitude of 6.0. Figure 5 illustrates how to perform the Physics-Based PSHA.

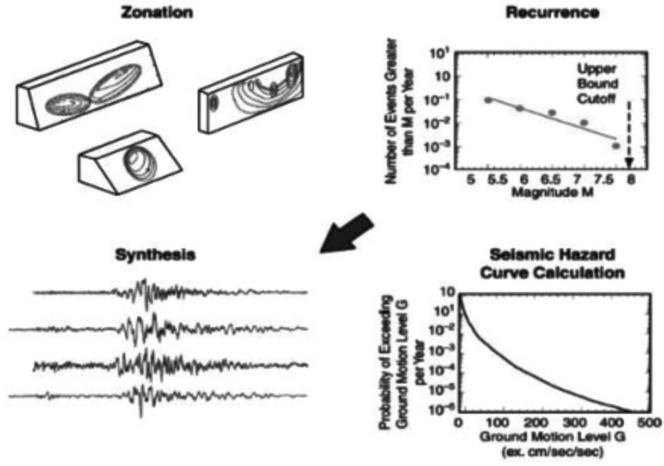

Figure 5. Steps in Physics-Based PSHA
Source: Hutchings and Viegas, 2012 [6]

Step 1 (Zonation). Fault sources are identified for earthquake rupture scenarios. Fault geometries are characterized for simulation of earthquakes. Uncertainties in the distance are not modeled any longer, but the distances are determined for wave propagation purposes.

Step 2 (Recurrence). Just like the conventional PSHA in Figure 3, magnitude occurrences are modeled to determine the recurrence parameters to predict a seismic hazard.

Step 3 (Synthesis). This is the difference with the conventional PSHA where the wave propagation from the fault rupture is simulated to create synthetic seismograms instead of the usual GMPEs. The fault rupture parameters such as fracture energy, stress drop, and rupture velocity to predict the ground motion are calculated.

Step 4 (Seismic Hazard Curve Calculations). This is similar to the conventional PSHA, where the predicted ground motion is paired up with the recurrence parameters that are linked to the magnitude occurrence, allowing the hazard analyst to construct the hazard curve.

Recent approaches by Tarbali et al. [19] and Tarbali et al. [20] make use of the software Cybershake for New Zealand which uses finite-fault rupture models by solving the 3D elastodynamic equation through a finite element method, and computing the hazard rate given by:

$$\lambda_{\mathfrak{I}}(\mathfrak{I}) = \sum_{n=1}^{N_{rup}} P_{\mathfrak{I} \vee Rup}(\mathfrak{I} \vee rup_n)\, \lambda_{Rup}(rup_n) \tag{6}$$

where $\lambda_{Rup}(ru\ p_n)$ is the hazard rate of a certain rupture scenario, and $P_{\mathfrak{I}\vee Rup}(\mathfrak{I}\vee ru\, p_n)$ is the probability of $\mathfrak{I} > \mathfrak{I}$ given $ru\, p_n$. This formulation does not need the uncertainty in the magnitude occurrence, but only the hazard rate obtained from the recurrence of earthquakes, such as the Guttenberg-Richter Law or Characteristic Earthquake models to be discussed in Section 4 of this paper. This formula is based on the probability of exceedance formulations of Field, Jordan, and Cornell [21] which abandons the integration of the seismic hazard rate from (2) with respect to the distance, magnitude, and sometimes the number of standard deviations when using (3).

1.3. Application to L'Aquila, Italy

For engineering applications such as the seismic design and retrofit of structures, it is of utmost importance to know the effects of the earthquake occurrence by estimating the seismic hazard in an area. As mentioned in the review of the seismic hazard zonation of Italy and other European countries in building codes for the seismic design, the reference peak ground acceleration (PGA) must conform to the 10% probability of being exceeded in 50 years of the design life of most structures [22].

According to Monaco et al. [3], the city of L'Aquila sustained a PGA of $0.65\boldsymbol{g}$ both for horizontal and vertical components. Wald et al. [23] formulated a relationship between the Modified Mercalli Intensity (MMI) Scale and PGA, and this PGA of $0.65\boldsymbol{g}$ may bring severe to violent ground shaking to the area which may bring moderate to heavy damage in an area. As shown in Figure 1, L'Aquila was devastated severely by this earthquake in 2009 and the city still has to recuperate from this as the city center is still under reconstruction.

The PSHA can estimate the underlying hazard in an area such as L'Aquila so that future earthquakes can be withstood by the structures to be constructed in the future, and the existing structures can be retrofitted. As per the previous PSHA in Central Italy by Valentini et al. [24], the PGA of L'Aquila corresponding to the 10% and 2% probability of exceedance in 50 years ranges between $0.225\boldsymbol{g}$ to $0.275\boldsymbol{g}$ and $0.60\boldsymbol{g}$ to $0.70\boldsymbol{g}$, respectively. This agrees with the PGA mentioned by Monaco et al. [3], making $0.65\boldsymbol{g}$ having a probability of exceedance of 2% in 50 years, or a return period of 2475 years. Their work is an improvement of another PSHA for the entire Italy of 2017 by Valentini, Visini, and Pace by considering the sequence of earthquakes during the 2016 Central Italy Earthquake the epicenter of which was located at Amatrice.

Hence, for the PSHA in L'Aquila, a non-ergodic assumption was employed for this paper since these two papers made use of the GMPEs from Italy and abroad, thus exhibiting the ergodic assumption. In general, this study aims to develop a PSHA Methodology by employing the non-ergodic assumption by solving the 1D elastodynamic equation to predict the PGA in L'Aquila. Specifically, this study aims to:

1. delineate all the seismic sources within 100 km from L'Aquila from the literature that can significantly contribute to the overall seismic hazard;

2. characterize all the seismic sources identified in this study in terms of their geometry, slip rates, style of faulting, activity rates, and location for earthquake rupture scenarios;
3. calculate distances to determine wave propagation lengths;
4. predict the PGA in all possible magnitude-distance pairs in all seismic sources by solving the 1D elastodynamic equation using staggered-grid finite differences;
5. calculate the hazard rates using the formulation of the seismic hazard (6); and
6. obtain the PGA values with a 10% and 2% probability of being exceeded in 50 years.

The assumptions of this study were as follows:

1. The PGA was assumed to occur at the bedrock level since this ground motion parameter could be modified by the type of soil (i.e. local amplification) which is beyond the scope of this paper;
2. The active fault sources described in these two papers were used extensively in this study by way of exchanging correspondence with Francesco Visini from INGV Pisa, one of the authors of both papers;
3. The active faults considered in this study were those located within a 100 km radius from the city of L'Aquila which could significantly contribute to the overall seismic hazard;
4. Seismic moment rates, mean the recurrence time, and some activity rates were obtained also from Francesco Visini;
5. The fault lines and coordinates were viewed using ArcGIS Pro. Also, the calculation of distances and the division of fault planes into equal areas were performed using ArcGIS Pro;
6. The minimum magnitude of occurrence considered in this study was 5.5 while the maximum was the M_{max} for each fault except for characteristic earthquake models where the minimum and maximum considered were $M_{max}\pm$ one standard deviation;
7. The distributed sources were not considered since the objective of this paper was to demonstrate the use of the Physics-based Ground Motion Prediction as smaller magnitudes were not considered in this study;
8. The Logic Tree Models to account for the epistemic uncertainty were not employed here since the fault parameters were available and GMPEs were not used, which was the advantage of studying L'Aquila as a site of interest;
9. For more conservative results, epicentral distances were obtained instead of hypocentral distances, assuming that the faults were found on the surface and not at a certain depth;
10. The body forces in the 1D elastodynamic equation were not considered;

11. A homogeneous medium was considered for the wave propagation from the source to the site;
12. The point-source approximation was employed as an implication of solving the 1D Elastodynamic Equation since only the PGA was important in the analysis of the ground motion and not the entire response as a function of time and space; and,
13. Hazard calculations were based on Tarbali et al. [19] and Tarbali et al. [20] being rupture-based scenarios, which for this study was the magnitude occurrence in the fault source. The probability of exceedances was computed based on the frequencies of the predicted PGA as a function of the distance given a magnitude of occurrence.

2. Engineering Seismology

In this Section some principles and theories will be discussed to describe the mechanism of the earthquake occurrence. Therefore, the basic notions of seismology relevant to engineering applications will be explained.

2.1. Seismic Waves and Earthquakes

Seismology is the study of earthquakes and movements of seismic waves in Earth's internal structure. When a geologic fault ruptures, an earthquake occurs and elastic strain energy is released through seismic waves which may affect ten to hundreds of kilometers. Seismic waves can be classified into two main types, namely *body waves* and surface waves [1].

Body waves are waves which can travel in the Earth's interior. The two main types of body waves are *p-waves* and *s-waves*. P-waves cause compression and rarefaction in the material along their axis when they pass through it. S-waves cause shearing in the material as they pass through it. While P-waves move parallel to the direction of travel, S-waves move perpendicular to the direction of travel. S-waves can be divided into two component waves, namely SH (pure horizontal motion) and SV (pure vertical motion) waves. Rocks are stiffest in compression, therefore, P-waves travel faster than S-waves, which reach the site faster [1]. The distinction between P-waves and S-waves for illustration is shown in Figure 6

Surface waves are formed when body waves interact with the uppermost layer of the earth. They travel along the surface of the earth, hence the name. There are two types of surface waves, namely *Rayleigh waves* and *Love waves*. Rayleigh waves are created when an SV wave interacts with a P-wave, while Love waves are created when an SH wave interacts with a soft layer of the Earth's surficial layer [1]. Figure 7 shows a comparison between Rayleigh and Love waves.

2.2. Faults

According to the Theory of Plate Tectonics, the surface of the Earth, which is composed of large, dense blocks floating over the viscous mantle which are

constantly moving with respect to each other [1]. This motion of plates causes deformation along boundaries, which produces earthquakes. This movement can be explained by *convection* in the mantle, which imposes shear stresses at the bottom of the plates. Due to these movements, new geologic structures are formed which are called *faults* or *geologic faults* in the form of cracks or discontinuities in the crust.

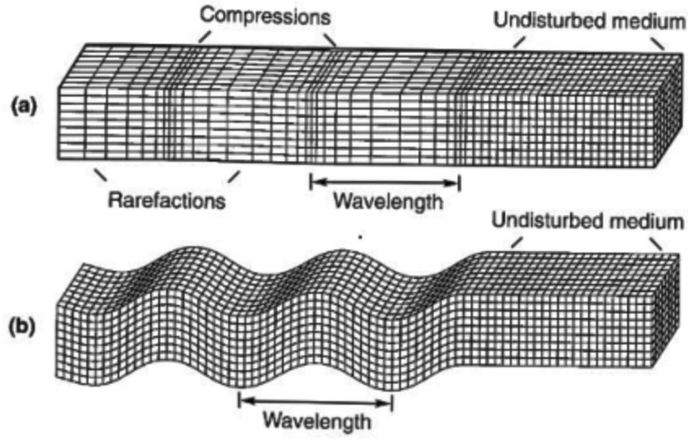

Figure 6. Material deformation caused by (a) P-wave (b) S-wave.
Source: Kramer, 1996 [1]

Faults can have a length ranging from several meters up to hundreds or thousands of kilometers, as in the case of the San Andreas Fault in the US. The presence of faults does not imply that an earthquake will occur in the future. For the purposes of a seismic hazard analysis, a fault must be active, which shows evidence of the fault activity in the late Quaternary or has evidence of the potential to be reactivated in the future [25]. The fault activity is characterized by recent slip displacements or slip rates in the past [1, 25].

2.2.1. Seismic source models

Generally, seismic sources can be modeled as a point, line, plane, or volume [26, 10, 27]. Usually, faults are area sources, which can be modeled as rectangular sources with length (L) along the ground surface or located at a certain depth (d_1) and width (W) which plunges beneath the earth surface. Refer to Figure 8 for visualization of a planar fault (or seismogenic box) as illustrated by Valentini, Visini, and Pace [25]. If a fault is too short in length and is too far from a site, it can be modeled as a point source. If the fault is near but it is short, it can be modeled as a line [1].

2.2.2. Fault Geometry

A fault can be described by the directions of its movement, namely the *strike* and the *dip*. The strike of a fault is the line which forms with the fault plane intersecting the horizontal plane. The azimuth of the strike (S) is the angle

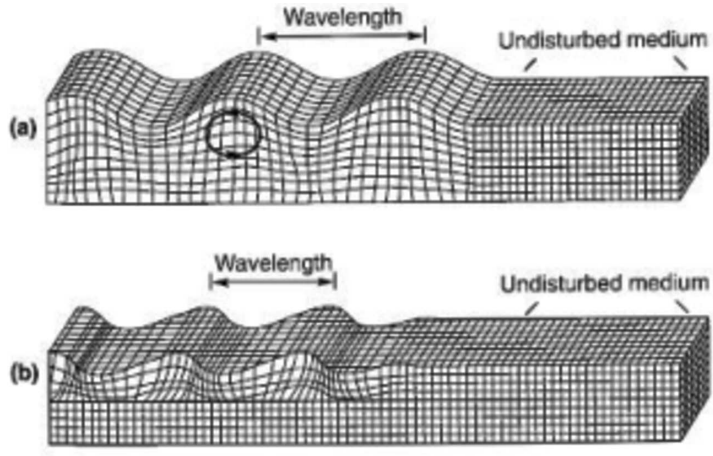

Figure 7. Material deformation caused by (a) Rayleigh wave (b) Love wave.
Source: Kramer, 1996 [1]

of this line relative to the North, usually measured from 0 to 360 degrees. The dip angle (θ) is the angle of the fault plane with the horizontal perpendicular to the strike. The geometric notation of faults is shown in Figure 8 [25] and Figure 9 [1].

Active faults are characterized by their sense of slip, or style of faulting [1]. Faults can be classified into *strike-slip* or *dip-slip faults*. If the dip angle of the fault is 90 degrees, then it is strike-slip. Otherwise, it is dip-slip. Furthermore, dip-slip faults are classified as *normal* or *reverse*. Normal faulting occurs when a hanging wall moves downward relative to the footwall. On the other hand, reverse faulting occurs when the hanging wall moves upward relative to the footwall [1]. In Italy, the majority of faults have this kind of style of faulting [25, 24].

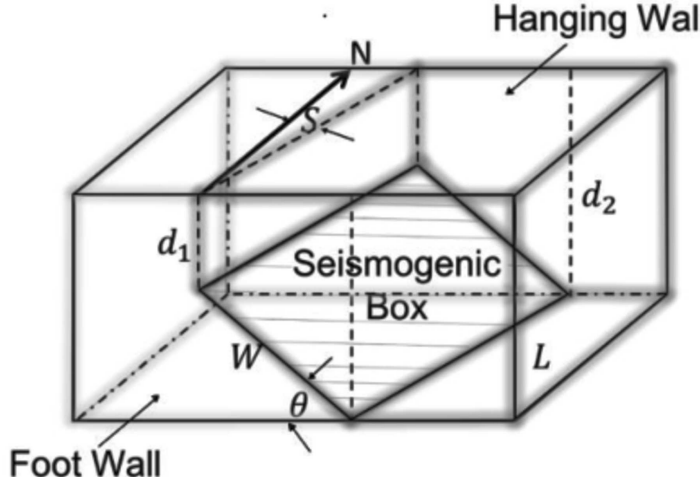

Figure 8. Geometric properties of a fault
Source: Valentini, Visini, and Pace, 2017 [25]

2.2.3. Geometric Notation of Earthquakes

In relation to the faults for which the seismic waves originate, the location of earthquakes is reported in terms of their distances from a seismic monitoring station. Figure 10 shows the different distances of an earthquake that can be described. The *epicentral distance* is the distance of the observer to the point on the ground surface projected above from the source of the tremor, which is called the epicenter. The source of the quake is called the *focus* or the *hypocenter* located along the fault plane. The distance of the observer to the focus is called the *hypocentral distance* [1].

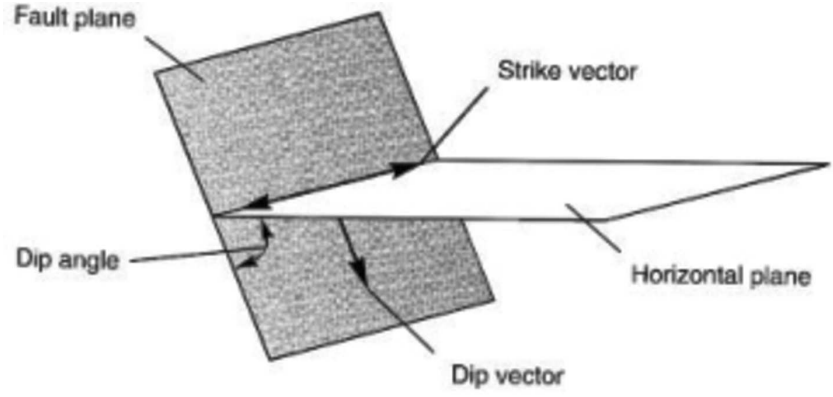

Figure 9. Geometric notation for fault orientation
Source: Kramer, 1996 [1]

2.3. Size of Earthquakes

The size of an earthquake refers to how small or big the impact of an earthquake is. This is important in any SHA as this parameter gives the audience what kind of earthquake to anticipate.

Intensity refers to the qualitative description of the an earthquake which differs from one place to another. This is subjective depending on the extent of the damage an earthquake does at a certain place. The *Modified Mercalli Intensity* (MMI) Scale is used to quantify the damage caused by an earthquake [1]. Cornell [10] pioneered the PSHA using the MMI Scale as the earthquake size, but changes have been made as intensity is qualitative only.

Magnitude is the size of an earthquake based on the amount of energy it has released. There are four main types of magnitude scales used: local (Richter), body-wave, surface-wave, and moment magnitude [1, 2, 28]. The first three scales mentioned above are obsolete nowadays for advanced countries, but these scales are still used, especially for developing countries. This is because these magnitude scales exhibit the *saturation effect* [28, 2, 1], or the inability of the scale to measure magnitudes beyond a certain value.

Nowadays, the moment magnitude scale is used to represent the size of an earthquake, especially in conducting a PSHA. This scale is based on the *seismic moment* of an earthquake when a geologic fault ruptures [29, 30]. The seismic moment M_0 (in dyne-cm) is given by:

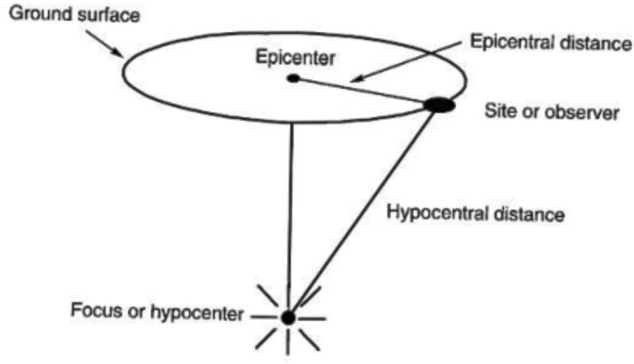

Figure 10. Geometric Notation of Earthquakes
Source: Kramer, 1996 [1]

$$M_0 = \mu AD \tag{7}$$

where μ is the shear modulus of rigidity of the rock equal to $3.3 \times 10^{10} \mathrm{N/m^2}$, A is the ruptured area of the fault (in square meters) and D is the average slip rate in the long run (in cm/yr). One may refer to Figure 8 to calculate the rupture area of the fault given the dip angle and the seismogenic thickness (or depth) of the fault. The moment magnitude M_w of an earthquake is given by [30]:

$$M_w = \frac{2}{3} \log M_0 - 10.7 \tag{8}$$

If the seismic moment is expressed in Newton-meters (N-m), the moment magnitude is given by [29].

$$M_w = \frac{2}{3} (\log M_0 - 9.1) \tag{9}$$

Since the moment magnitude scale is based on the seismic moment, it is a very good measurement of the size of an earthquake [1, 28, 2]. Therefore, the moment magnitude scale is typically the magnitude scale used in conducting a PSHA.

Other relations are correlated by Causse, Dalguer, and Mai [31] to relate the seismic moment (in N-m) to the dynamic stress drop ($\triangle\sigma_d$) and the fracture energy (G) during earthquakes are given by:

$$\begin{aligned} \log \triangle\sigma_d &= 0.21 \log M_0 - 3.0 \\ \log G &= 0.60 \log M_0 - 10.6 \end{aligned} \tag{10}$$

The stress drop is the decrease in shear stresses in rocks after a fault ruptures, while the fracture energy is the energy required to initiate fracture in rocks [32].

Given these relationships between the seismic moment, the moment magnitude, the dynamic stress drop and the fracture energy, an earthquake for the seismic hazard analysis can be simulated.

2.4. Elastic Rebound Theory

As plates move toward each other, elastic strain energy builds up along the edges of the two plates in motion. This energy continues to build up until such time that the shear strength of rocks is exceeded, and thus rupture occurs (and subsequently, the earthquake occurs) and the energy is released. The nature of failure of rocks depends on the type of material of the rock. If the rock is brittle and strong, it is expected to have a sudden release of energy which can be transformed into some heat and some shear waves. If the rock is ductile and weak, only small energy is released and therefore faults move slowly and will not cause a massive earthquake [1]. This process of building up the elastic strain energy and releasing the energy to the rock next to the fault is called the *Elastic Rebound Theory*. Figure 11 shows the two possible failure modes of rocks along the fault line.

Not all earthquakes reported by a seismic monitoring station result from a sudden release of strain energy in rocks. These earthquakes can be classified as *foreshocks, main shocks*, or *aftershocks*. The elastic rebound theory can explain the difference between these three shocks. The energy stored and the strength distributed along the fault are not the same, meaning that certain portions of rocks are relatively weaker. In cases where a weaker portion ruptures, a foreshock will occur. These kinds of earthquakes will occur until the strongest part of the fault, also known as *asperity*, ruptures, and this will trigger the occurrence of the main shock. Then, after some time, some remaining stronger portions of the fault will have their shear strengths exceeded upon a continuous movement of the crust, and this will trigger the occurrence of aftershocks [1].

As mentioned by Kramer [1], the elastic rebound theory states that the occurrence of earthquakes will de-stress the fault until new elastic energy builds up again. This implies that all the earthquakes attributed to a ruptured fault are not random and dependent on each other. The knowledge of this concept is very important in the PSHA particularly in modeling the occurrence of earthquakes.

2.5. Seismograms

The ground motion on a certain site during an earthquake excitation is measured by instruments called *seismographs* or *accelerographs* and the recordings are plotted on *seismograms* or *accelerograms*, or which shows the variation of displacement, velocity, or acceleration as a function of time [1]. Figure 12 shows an example of a typical seismogram.

Seismograms are used in creating *response spectra* by taking the Fourier Transform of the displacement, velocity, or acceleration to produce a plot of maximum response values of ground motion parameters (displacement, velocity, or acceleration) of structures and soils as a function of *natural period*, a property

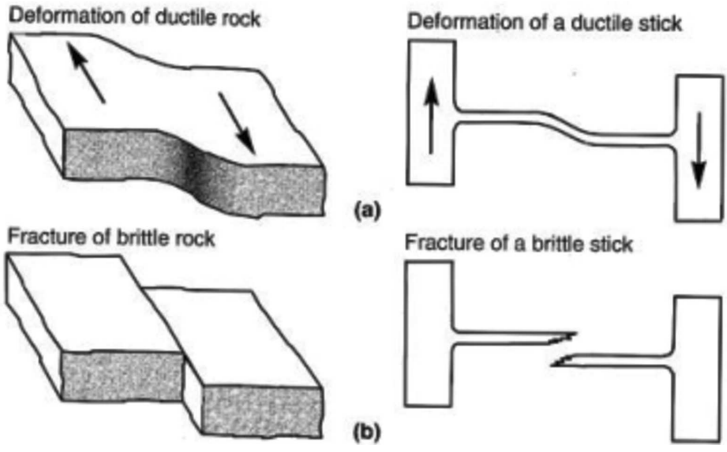

Figure 11. Failure modes of rocks along the fault: (a) ductile (b) brittle
Source: Kramer, 1996 [1]

of a structure or soil which is the time that it takes for the structure or soil to complete an oscillation [1]. This is a very important application of seismograms for engineering purposes.

Seismograms are also used to characterize an earthquake in terms of its peak ground acceleration (PGA), peak ground velocity (PGV), or peak ground displacement (PGD). As mentioned before, PGA is important for building code applications [22, 1].

For seismic hazard applications, a seismogram can be created synthetically by performing a numerical simulation of the earthquake mechanism if the style of faulting, the magnitude, and the rock properties are known [18, 6, 33].

2.6. Ground Motion Prediction Equations

It is indeed a vital part for any seismic hazard analysis to model the behavior of seismic waves as they travel from one place to another. Predictive relations that relate the ground motion to the magnitude, distance and other parameters are called *Ground Motion Prediction Equations (GMPE)* or *Attenuation Relationships* [2, 10, 14, 1, 27]. Usually, a GMPE takes the form of the expression shown in (5).

2.6.1. Statistical Approach

According to Kramer [1], the function must reflect the mechanics of the ground motion as exactly as possible, hence, the available strong ground motion data in the form of time histories is used to correlate the ground motion parameters and the magnitude and distance of the occurrence, considering the soil type and the style of faulting. Usually, GMPEs are expressed in terms of the natural logarithm of the ground motion parameter since the logarithms of the ground motion parameter are normally distributed, as shown in (5). Equation (11) elaborates the expressions of a GMPE used in the study of Landwehr, et al. [13]:

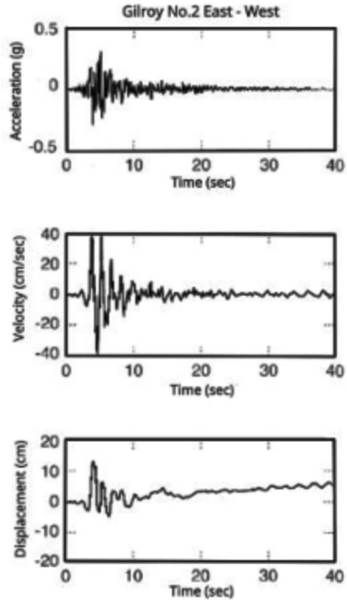

Figure 12. An accelerogram obtained from Gilroy Site, with velocity and displacement time histories integrated using the Trapezoidal Rule.
Source: Kramer, 1996 [1]

$$y = \beta_0 + \beta_1 M + \beta_2 M^2 + (\beta_3 + \beta_4 M) \ln \sqrt{R_{JB}^2 + h^2} + \\ + \beta_5 R_{JB} + \beta_6 \ln V_{S30} + \beta_7 F_R + \beta_8 F_{NM} + \epsilon \tag{11}$$

where $y = y(M, R_{JB}, V_{S30}, F)$ is the ground motion parameter of interest, β_i are the coefficients to be determined, M is the magnitude, R_{JB} is the nearest distance from the source to the site projected vertically upward, V_{S30} is the shear wave velocity in the uppermost 30 m height of soil on the site, F takes account of the style of faulting (reverse or normal fault), h is a constant and ϵ s a residual term. These coefficients are to be determined given a strong ground motion data set.

Since the equation is a result of regression, an error term also known as the *uncertainty* in the ground motion parameter is always present, usually expressed as a standard deviation of the natural logarithm of the ground motion parameter. This uncertainty makes the use of GMPEs to be an ergodic approach, which assumes that data measurements that are spatially varying are the same as sampling as a function of time at a single point in space [12]. For a PSHA to have fewer uncertainties, the new focus of studies is currently a non-ergodic assumption which deals with improvement of GMPEs.

According to Anderson and Brune [12] and Landwehr et al. [13], this uncertainty in the GMPEs can be broken down into two main components: the aleatory uncertainty (or variability), which represents the randomness in the ground motion and is inherent to the ground motion; and the epistemic

uncertainty, which accounts for the lack of knowledge in the process of the earthquake occurrence and the lack of data.

Landwehr et al. [13] tried to minimize the aleatory variability in their studies by considering the repeatability of measurements to account for the epistemic uncertainties in the path, source, and site of interest, making these uncertainties distributed into multiple points across California. These resulted in a decrease in the aleatory variability by 40% and a decrease in the epistemic uncertainty in areas with more data, but an increase in areas with scarce data.

Kotha, Bindi, and Cotton [16] shifted their PSHA from an ergodic assumption to a regional and site specific PSHA, minimizing the overall hazard as much as 25% in a regional PSHA and as high as 50% change in a site specific environment.

2.6.2. **Physics-Based Approach**

The problem in the ergodic assumption in the PSHA is the treatment of both the aleatory and epistemic uncertainties. Using this approach, a correlation between the ground motion and the specific source, path is lost which results in building the uncertainties [18, 6]. In this regard, there is a need for more data regarding historical earthquakes to be more certain of an earthquake process. Thus, employing an actual physical model with physical parameters of the fault can be used to characterize the actual ground motion itself, while keeping the original characteristics of the seismic source that produced that earthquake. The aim of the physics-based approach is to produce a library of ground motions which are site-specific and source-specific, which is also done in a normal DSHA or PSHA by classifying the site and seismic sources for the GMPE to be utilized. In this way, too much uncertainty in the ground motion can be avoided to be incorporated into the seismic hazard. Incorporating this deterministic approach into a probabilistic framework not only justifies using a model of an actual earthquake, but it also gives meaning to the inherent randomness of an actual process.

The wave propagation from a seismic source is governed by the *Elastodynamic Equation* which is given by [17]:

$$\rho \ddot{u}_i = f_i + \tau_{ij,j} \tag{12}$$

where ρ (assumed constant) is the volumetric mass density of the deforming body, $\boldsymbol{u} = (u_1, u_2, u_3) \in \mathbb{R}^3$ is the displacement vector, $\boldsymbol{f} = (f_1, f_2, f_3) \in \mathbb{R}^3$ is the body force vector, and $\tau_{ij,j} \in \mathbb{R}^3$ is the Cauchy Stress tensor, with j subscript indicating a spatial derivative with respect to coordinate j, and the dot represents the time derivative. The result of solving the elastodynamic equation is a synthetic seismogram, which can be used to predict the ground motion [34, 17, 33].

Equation (11) is a partial differential equation in time and space, which requires another relationship from the properties of the material to solve it, provided that the initial and boundary conditions are satisfied. This equation will be derived in the next Section.

2.7. Derivation of Elastodynamic Equation

The derivation from Aki and Richards [17] will be discussed here. There are two ways to fully express kinematics and kinetics in a continuum. The *Lagrangian coordinates* are used to study a particle of interest with the known starting position at a given time frame, and the *Eulerian coordinates* are used to study any particle moving along in any time and space. For seismology applications, it is better to describe the motion of particles in Lagrangian coordinates since seismograms are site-specific and are studied at a given location and time.

In this paper, the Cartesian Coordinate system will be used, and the tensors are also Cartesian. Let $\boldsymbol{u}=\boldsymbol{u}(\boldsymbol{x},t)$ be the displacement as a function of position $\boldsymbol{x}\in\mathbb{R}^3$ and time $t\in[0,T]$, where T is the duration of an earthquake. Let this position be taken at a certain reference time $t=0$. Denote the *particle velocity* as $\dot{\boldsymbol{u}}=\partial\boldsymbol{u}/\partial t$ and the *particle acceleration* as $\ddot{\boldsymbol{u}}=\partial^2\boldsymbol{u}/\partial^2 t$. Hence, the regularity required for $\boldsymbol{u}$ is C^2 in time. It must be assumed also for now that $\boldsymbol{u}$ is C^1 in space.

If a particle with initial position x traveled to a point with new position $\boldsymbol{x}+\boldsymbol{u}$, then $\boldsymbol{u}\equiv\boldsymbol{u}(\boldsymbol{x})$ is the displacement field. Let $\delta\mathbf{x}$ be a deformation introduced on a portion of a medium the position of which is $\boldsymbol{x}$ such that the particle position is initially at $\boldsymbol{x}+\delta\boldsymbol{x}$. Then, the new position of the particle becomes $\boldsymbol{x}+\delta\boldsymbol{x}+\boldsymbol{u}(\boldsymbol{x}+\delta\boldsymbol{x})$. Any deformation is responsible for changing the relative position of the endpoints of line-element $\delta\boldsymbol{x}$. If the change is $\delta\boldsymbol{u}$, then the new vector line-element corresponds to $\delta\boldsymbol{x}+\delta\boldsymbol{u}$ which is equivalent to:

$$\delta\boldsymbol{x}+\delta\boldsymbol{u}=\boldsymbol{x}+\delta\boldsymbol{x}+\boldsymbol{u}(\boldsymbol{x}+\delta\boldsymbol{x})-(\boldsymbol{x}+\boldsymbol{u}(\boldsymbol{x})) \tag{13}$$

For $|\delta\mathbf{x}|$ very small $\mathbf{u}(\mathbf{x}+\delta\mathbf{x})$ can be approximated by the first order Taylor Series expansion as

$$\boldsymbol{u}(\boldsymbol{x}+\delta\boldsymbol{x})\approx\boldsymbol{u}(\boldsymbol{x})+(\delta\boldsymbol{x}\cdot\nabla)\,\boldsymbol{u}(\boldsymbol{x})+O\left(|\delta\boldsymbol{x}|^2\right) \tag{14}$$

By inspection, it follows that

$$\delta\boldsymbol{u}=(\delta\boldsymbol{x}\cdot\nabla)\,\boldsymbol{u}\qquad\text{or}\qquad\delta u_i=\frac{\partial u_i}{\partial x_i}\delta x_j \tag{15}$$

First, let the spatial derivative be denoted by $u_{i,j}=\partial u_i/\partial x_i$ and let the Kronecker symbol $\delta_{i,j}$ and the alternating tensor with components ε_{ijk} be denoted as:

$$\delta_{ij}=\begin{cases}1 & if\quad i=j\\ 0 & if\quad i\neq j\end{cases}\qquad\varepsilon_{ijk}=\begin{cases}1 & if\quad (i,j,k)=(1,2,3),(2,3,1),(3,1,2)\\ 0 & if\quad i=j=k\\ -1 & otherwise\end{cases} \tag{16}$$

Also, the important properties of these notations are

$$a_i=\delta_{ij}a_j\qquad\text{and}\qquad\varepsilon_{ijk}a_jb_k=(\boldsymbol{a}\times\boldsymbol{b})_i \tag{17}$$

and these are also associated with the following properties:

$$\varepsilon_{ijk}\varepsilon_{ilm} = \delta_{jl}\delta_{km} - \delta_{jm}\delta_{kl} \qquad \text{and} \qquad \varepsilon_{ijk}\varepsilon_{lmn} = \begin{vmatrix} \delta_{il} & \delta_{jl} & \delta_{kl} \\ \delta_{im} & \delta_{jm} & \delta_{km} \\ \delta_{in} & \delta_{jn} & \delta_{kn} \end{vmatrix} \tag{18}$$

Since a part of the motion is caused only by an infinitesimal rigid-body rotation about $\boldsymbol{x}$, it is not a prerequisite to solve for all the nine independent components of the tensor $u_{i,j}$. Using the properties from (16)- (18) and the identity $(u_{i,j} - u_{j,i})\delta x_j = \varepsilon_{ijk}\varepsilon_{jlm}u_{m,l}\delta x_k$, (15) can be rewritten as

$$\delta u_i = \frac{1}{2}\left(u_{i,j} + u_{j,i}\right)\delta x_j + \frac{1}{2}\left(\text{curl } \boldsymbol{u} \times \delta\mathbf{x}\right)_i \tag{19}$$

with the rigid-body rotation equal to curl $\boldsymbol{u}$, and the last term of (19) can be viewed as rigid-body rotation if and only if $|u_{i,j}| \ll 1$. Then, define the strain tensor with the components

$$e_{ij} = \frac{1}{2}\left(u_{i,j} + u_{j,i}\right) \tag{20}$$

the effect of true deformation on any line-element δx_j, making the change to the relative position to its endpoints by $e_{ij}\delta x_j$. Since the rigid-body motion does not impose deformation, hence, the new length is given by:

$$\begin{aligned} |\delta\boldsymbol{x} + \delta\boldsymbol{u}| &\approx \sqrt{\delta\boldsymbol{x}\cdot\delta\boldsymbol{x} + 2\delta\boldsymbol{u}\cdot\delta\boldsymbol{x}} && \text{(neglecting } \ \delta\boldsymbol{u}\cdot\delta\boldsymbol{u}) \\ &= \sqrt{\delta x_i \cdot \delta x_i + 2e_{ij}\delta x_i \delta x_j} && \text{(using (19) and since (curl } \boldsymbol{u}\times\delta\boldsymbol{x})\cdot\delta\mathbf{x} = 0) \\ &\approx |\delta\boldsymbol{x}|\left(1 + e_{ij}\gamma_i\gamma_j\right) && \text{(binomial approx. to first order, if } |e_{ij}| \ll 1) \end{aligned}$$

where $\boldsymbol{\gamma}$ is the unit vector $\delta\boldsymbol{x}/|\delta\boldsymbol{x}|$. Hence, the extension imposed by deformation $\delta\boldsymbol{u}$ is directed towards $\boldsymbol{\gamma}$ is equal to $e_{ij}\gamma_i\gamma_j$. This result will be used later for the material property to solve (12).

Now, the internal forces acting on the particles of the continuum must be identified, and for that purpose the concepts of *traction* and *stress tensor* will be used. These forces are called surface or *contact forces*. Traction is the vector of force per unit area acting on an internal surface S with normal $\boldsymbol{n} \in \mathbb{R}^3$ on the continuum as shown in Figure 13a. This force denoted by $\delta\boldsymbol{F} \in \mathbb{R}^3$ can act as an angle with respect to $\boldsymbol{n}$, such that these two vectors are not parallel. This is possible for solids, for which shear stresses can act. For a given point on S, traction $\boldsymbol{T} \in \mathbb{R}^3$ is defined as the infinitesimal force $\delta\boldsymbol{F}$ acts along the infinitesimal surface δS, and taking the limit $\delta\boldsymbol{F}/\delta S$ as $\delta S \to 0$. This traction acts as if the material is being pulled to the normal points, and so the traction is $\boldsymbol{T} = \boldsymbol{T}(\boldsymbol{n})$.

Next, the forces existing among the particles and other forces resulting from some physical phenomenon outside the medium must be taken into account. These are called body forces such as gravitational and magnetic forces, which can be denoted by $\boldsymbol{f}(\boldsymbol{x}, \boldsymbol{t}) \in \mathbb{R}^3$ to indicate the body forces per unit volume at an initial

position $\boldsymbol{x}$ and a certain initial time frame. Usually, it is preferable to have body forces to be applied impulsively (or a very large force applied at a very short time) to a specific particle $\boldsymbol{x}=\boldsymbol{\xi}$ and $t=t_0$. This force, component-wise, is proportional to the Dirac Delta Function $\delta(\boldsymbol{x}-\boldsymbol{\xi})$ in space, the Dirac Delta Function $\delta(t-t_0)$ in time, and the Kronecker Delta function $\delta(t-t_0)$, which indicates directionality that $f_i=0$ fot $i\neq n$. Then, combining these assumptions, the body force is given by:

$$f_i(\boldsymbol{x},t)=A\delta(\boldsymbol{x}-\boldsymbol{\xi})\delta(t-t_0)\delta_{in} \tag{21}$$

where $A\in\mathbb{R}$ is the strength of the impulse. To analyze the dimension, f_i, $\delta(\boldsymbol{x}-\boldsymbol{\xi})$, and $\delta(t-t_0)$ have the dimensions of force per unit volume, 1/unit volume and 1/unit time, hence, A has a dimension of force x time which is the same for an impulse.

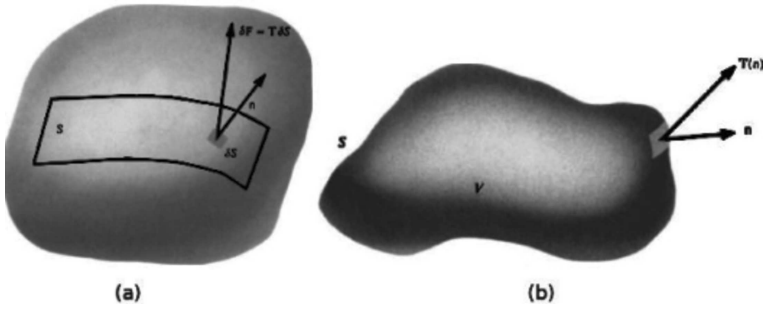

Figure 13. (a) Traction acting on internal surface S
(b) volume material V of the continuum with surface S
Source: Aki and Richards, 2002 [17]

Consider volume V of the material with surface S in Figure 13b. By Newton's Second Law of Motion, the change in momentum in the entire volume V is the sum of the body forces and the traction. Mathematically, this is given by:

$$\frac{\partial}{\partial t}\int\limits_V \rho\frac{\partial \boldsymbol{u}}{\partial t}dV=\int\limits_V \boldsymbol{f}dV+\int\limits_S \boldsymbol{T}(\boldsymbol{n})dS \tag{22}$$

with V and S moving along with the particles. Since V does not depend on time, the time derivative can be put inside the integral making (22) equivalent to:

$$\int\limits_V \rho\frac{\partial^2 \boldsymbol{u}}{\partial t^2}dV=\int\limits_V \boldsymbol{f}dV+\int\limits_S \boldsymbol{T}(\boldsymbol{n})dS \tag{23}$$

Now, consider a small tetrahedron (as shown in Figure 14) with three of its faces lying along the coordinate axes with outward normals $\hat{x}_j$ $(j=1,2,3)$, while the fourth face has a normal $\boldsymbol{n}$. To arrive at (11) the first step is to find a good expression for the traction. To accomplish this, consider a particle P within the medium located in the origin with distance $\epsilon\to 0$ from the corners of the tetrahedron. Also, assume that $\partial^2\boldsymbol{u}/\partial t^2$, $\boldsymbol{f}$, $\boldsymbol{T}$ are C^1 functions. Then, it follows

that $|V| \sim \epsilon^3$ and $|S| = |\partial V| \sim \epsilon^2$. The expressions in the volume integrals can be bounded by their maximum values as shown:

$$\int_V \rho \frac{\partial^2 \boldsymbol{u}}{\partial t^2} dV \leq \rho \left| \frac{\partial^2 \boldsymbol{u}}{\partial t^2} \right| |V| \qquad \int_V \boldsymbol{f} dV \leq |\boldsymbol{f}||V| \tag{24}$$

It can be observed from (23) that all the terms have the same units of forces, with the traction terms composed of the traction multiplied by the area. Combining the terms in (24) in the left-hand side and dividing everything with the measure of S, one can obtain:

$$\frac{|V|}{|S|} \left[\rho \left| \frac{\partial^2 \boldsymbol{u}}{\partial t^2} \right| - |\boldsymbol{f}| \right] = \frac{\left| \int_S \boldsymbol{T} dS \right|}{|S|} \tag{25}$$

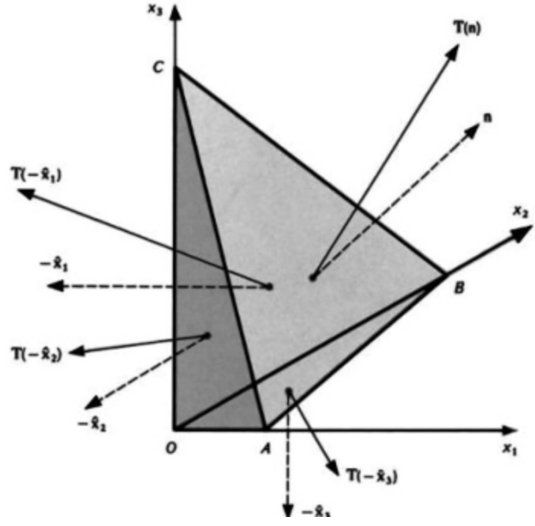

Figure 14. Infinitesimal tetrahedron given the faces and their respective normal outward vectors.
Source: Aki and Richards, 2002 [17]

Since $|V|$ has the measure ϵ^3 and $|S|$ has the measure ϵ^2, it follows that $|V|/|S| \sim \epsilon \to 0$ and thus, the left-hand side of (25) approaches zero, forcing the right-hand side also to approach zero as $\epsilon \to 0$ and thus one obtains:

$$\frac{\left| \int_S \boldsymbol{T} dS \right|}{|S|} \to 0 \tag{26}$$

The second step is to consider that V is an infinitesimal cylinder with height ϵ and radius ϵ, whose bases are centered at $\boldsymbol{x}$, as shown in Figure 15. It is desirable to

show that $\boldsymbol{T}(-\boldsymbol{n}) = -\boldsymbol{T}(\boldsymbol{n})$. Then, the integral term in (22) involving the traction for the cylinder in Figure 15 is given by:

$$\int_S \boldsymbol{T} dS = \int_{B_1} \boldsymbol{T}(\boldsymbol{n}(\mathbf{x}))\, dS + \int_{B_2} \boldsymbol{T}(-\boldsymbol{n}(\boldsymbol{x}))\, dS + \int_{B_3} \boldsymbol{T}\left(\boldsymbol{n}_{B_3}(\boldsymbol{x})\right) dS \tag{27}$$

By the mean value theorem for integrals, for some $\boldsymbol{x}_{B1}, \boldsymbol{x}_{B2}, \boldsymbol{x}_{B3} \in V$ and $\boldsymbol{T}(\boldsymbol{n})$ continuous on V, one has:

$$\int_S \boldsymbol{T} dS = |B_1| \left| \boldsymbol{T}\left(\boldsymbol{n}(\boldsymbol{x}_{B_1})\right) \right| + |B_2| \left| \boldsymbol{T}\left(-\boldsymbol{n}(\boldsymbol{x}_{B_2})\right) \right| + |B_3| \left| \boldsymbol{T}\left(\boldsymbol{n}(\boldsymbol{x}_{B_3})\right) \right| \tag{28}$$

It follows from the cylinder in Figure 15 that $|V| = \pi\epsilon^4$ and $|\mathrm{S}| = 2^3 + 2\pi\epsilon^2 \approx 2\pi\epsilon^2$ and due to (26), dividing (28) by $|S|$ yields:

$$\frac{1}{|S|} \int_S \boldsymbol{T} dS = \frac{|B_1|}{|S|} \left| \boldsymbol{T}\left(\boldsymbol{n}(\boldsymbol{x}_{B_1})\right) \right| + \frac{|B_2|}{|S|} \left| \boldsymbol{T}\left(-\boldsymbol{n}(\boldsymbol{x}_{B_2})\right) \right| + \frac{|B_3|}{|S|} \left| \boldsymbol{T}\left(\boldsymbol{n}(\boldsymbol{x}_{B_3})\right) \right| \tag{29}$$

and setting $\epsilon \to 0$, $\boldsymbol{x}_{B_1}, \boldsymbol{x}_{B_2}, \boldsymbol{x}_{B_3} \to \boldsymbol{x}$ and the cylinder will be squeezed to $\boldsymbol{x}_{B_1}, \boldsymbol{x}_{B_2}, \boldsymbol{x}_{B_3}$ which results in:

$$0 = \frac{1}{2} \boldsymbol{T}(\boldsymbol{n}(\boldsymbol{x})) + \frac{1}{2} \boldsymbol{T}(-\boldsymbol{n}(\boldsymbol{x})) \tag{30}$$

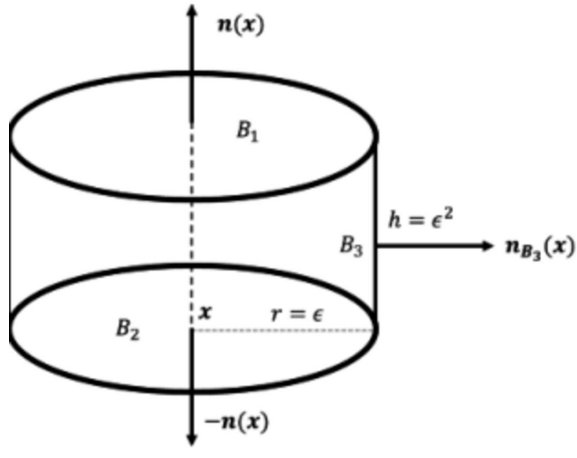

Figure 15. An infinitesimal cylinder centered at $\mathbf{x}$ with normal $\boldsymbol{n}(\boldsymbol{x})$ and $-\boldsymbol{n}(\boldsymbol{x})$ along surfaces B_1 and B_2, normal $\boldsymbol{n}_{B_3}(\boldsymbol{x})$ along surface B_3.

with the third term becomes $\epsilon\, \boldsymbol{T}\left(\boldsymbol{n}_{B_3}(\boldsymbol{x})\right) \to 0$ as $\epsilon \to 0$. And thus, it is shown that:

$$\boldsymbol{T}(-\boldsymbol{n}) = -\boldsymbol{T}(\boldsymbol{n}) \tag{31}$$

The third step is to go back to Figure 14. As a consequence of (26), it is implied that:

$$\frac{\boldsymbol{T}(\boldsymbol{n})|ABC| + \boldsymbol{T}(-\hat{\boldsymbol{x}}_1)|OBC| + \boldsymbol{T}(-\hat{\boldsymbol{x}}_2)|OCA| + \boldsymbol{T}(-\hat{\boldsymbol{x}}_1)|OAB|}{|ABC| + |OBC| + |OCA| + |OAB|} \to 0 \tag{32}$$

as $\epsilon \to 0$. Moreover, one can show that the components of the normal vector $\boldsymbol{n}$ are given by $(n_1, n_2, n_3) = (|OBC|, |OCA|, |OAB|)/|ABC|$. To show this, the Gauss Divergence theorem can be used. Assuming that for $n_i > 0$, we have:

$$0 = \int_V div\ \hat{\boldsymbol{x}}_{\boldsymbol{j}} dV = \int_{ABC} \hat{\boldsymbol{x}}_{\boldsymbol{j}} \cdot \boldsymbol{n}\, dS - \sum_{i=1}^{3} \int_{B_1} \hat{\boldsymbol{x}}_{\boldsymbol{i}} \cdot \hat{\boldsymbol{x}}_{\boldsymbol{j}}\, dS = n_j |ABC| - |B_i|$$

where B_i are areas $(|OBC|, |OCA|, |OAB|)$. Hence, from (32) and (31), one can obtain

$$\mathbf{T}(\mathbf{n}) = \mathbf{T}(\hat{\mathbf{x}_\mathbf{j}})\, n_j \tag{33}$$

Defining the stress tensor with components $\tau_{kl} = T_l(\hat{x}_k)$ so that τ_{kl} is the lth component of the contact stress acting on the plane normal to the kth axis with the above material acting upon another material below. Hence, using this definition one has:

$$T_i = \tau_{ji} n_j \tag{34}$$

Using Figure 14 and the result from (34), the equation of motion of a general particle can be studied. Using the Gauss Divergence Theorem, (34) yields,

$$\int_S T_i dS = \int_S \tau_{ji} n_j dS = \int_V \tau_{ji,j} dV \tag{35}$$

and the volume of the material can be generalized such that from (23), one has

$$\int_V \left(\rho \frac{\partial^2 u_i}{\partial t^2} - f_i - \tau_{ji,i} \right) dV = 0 \qquad \blacksquare \tag{36}$$

which is our desired result. The integral in (36) is zero for any choice of volume V with the assumption that the acceleration, body forces, traction are continuous functions on V.

For simplicity in solving, only one-dimensional elastodynamic equation was considered in this study since the fault models used in this study are simple fault models and the PSHA employed in this study considers the classical approach of obtaining distances of discretized seismic sources, which is similar to using GMPEs that require a single distance. Hence, (12) can be simplified for a 1D case and is given by

$$\rho \frac{\partial^2 u}{\partial t^2} = f + \frac{\partial \tau}{\partial x} \tag{37}$$

According to Shearer [32], the body force does not dominate in regions of the earth that are far away from the source, and for the purpose of solving (37), the body force was not considered in this study and the homogenous equation was used:

$$\rho \frac{\partial^2 u}{\partial t^2} = \frac{\partial \tau}{\partial x} \tag{38}$$

It can be noticed that there are two variables of interest here: the displacement and the traction. This equation alone cannot be solved even if there are enough

boundary conditions, hence, a *constitutive* relation coming from the property of the medium must be used to solve (37). This property of material involves the relationship between the stress and the strain in a perfectly elastic medium, which is called the *Hooke's Law*[1], and is given for one-dimensional case by:

$$\tau = \mu e_{ii} = \frac{\mu}{2}\left(u_{i,i} + u_{i,i}\right) = \mu \frac{\partial u}{\partial x} \tag{39}$$

where e_{ii} is the strain tensor for one dimension from (20) and μ s a Lamè constant also known as the shear modulus of rigidity. To avoid expressions of a second-order term in (37), the velocity response can be used instead by introducing $\nu = \partial u/\partial t$ and taking the time derivative in (38), which yields into a system of two PDEs given by:

$$\begin{cases} \rho \frac{\partial \nu}{\partial t} = \frac{\partial \tau}{\partial x} \\ \\ \frac{\partial \tau}{\partial t} = \mu \frac{\partial \nu}{\partial x} \end{cases} \tag{40}$$

and this system of PDEs form a second-order linear PDE which will be discussed further in the next Section.

3. Wave Equation

In this Section, the elastodynamic equation will be treated mathematically by studying partial differential equations, the well-posedness of the problem, and numerical solution of the elastodynamic equation.

3.1. Partial Differential Equations

A partial differential equation (PDE) is a type of equation involving an unknown function of two or more variables [35]. In this Section, all concepts regarding PDEs will be focused on one-dimension only.

3.1.1. **Preliminaries**

Definition 1. The PDE that can be expressed as

$$F\Big(D^k(\boldsymbol{x}), D^{k-1}u(\boldsymbol{x}), ..., D\,u(\boldsymbol{x}), u(\boldsymbol{x}), \boldsymbol{x}\Big) = 0 \qquad (\boldsymbol{x} \in V) \tag{41}$$

is called a k-*th* order PDE, where $F: \mathbb{R}^{n^k} \times \mathbb{R}^{n^{k-1}} \times ... \mathbb{R}^n \times \mathbb{R} \times V \to \mathbb{R}$ is given, while the function $u: V \to \mathbb{R}$ is the unknown variable and U is a vector space with x a vector of some dimension d.

1. For 3-D, Hooke's Law is expressed as $\tau_{ij} = c_{ijpq} e_{pq}$ with c_{ijpq} is a fourth-degree tensor with symmetries $c_{ijpq} = c_{ijpq}$ and $c_{ijpq} = c_{ijpq}$ due to $\tau_{ij} = \tau_{ij}$ and $e_{pq} = e_{pq}$ respectively. See Aki and Richards [17]

The notation $D^k u$ means that the function is differentiated k times with respect to two or more variables, depending on the dimension of U . In the usual partial derivative notation,

$$D^k u = \frac{\partial^k u}{\partial x_1^{\alpha_1} \partial x_2^{\alpha_2} ... \partial x_d^{\alpha_d}} = u_{\underbrace{x_1 x_1 ... x_1}_{\alpha_1 \text{times}} \underbrace{x_2 ... x_2}_{\alpha_2 \text{times}} ... x_d ... x_d}$$

where $\sum_i \alpha_i = k$ and x_i are components of $\boldsymbol{x} = (x_1, ..., x_d)$.
The PDE (41) is solved if all the possible functions are obtained and found to satisfy (41) given a number of additional boundary conditions along the boundary ∂V. The solution means a simple, straightforward expression that satisfies (41), or showing the existence of solutions and their properties.

Definition 2. The PDE in (41) is said to be of a linear type if it can be expressed as

$$\sum_{|\alpha| \le k} a_\alpha(x) D^\alpha u = f(x)$$

for given functions $a_\alpha (|\alpha| \le k)$, f. Also, this PDE is said to be homogeneous if $f \equiv 0$. The PDE in (41) is said to be of a *semi-linear* type, the principal part only, the one with the highest order, is linear, and the other expressions of partial derivatives of lower order are nonlinear. The PDE is *quasilinear* if the function multiplied to the principal part is nonlinear, but the highest derivative term remains linear. If none of these three classify as a PDE, then it is *nonlinear*.

Definition 3. The PDE in the form of

$$\boldsymbol{F}\Big(D^k \boldsymbol{u}(\boldsymbol{x}), D^{k-1} \boldsymbol{u}(\boldsymbol{x}), ..., D\, \boldsymbol{u}(\boldsymbol{x}), \boldsymbol{u}(\boldsymbol{x}), \boldsymbol{x}\Big) = 0 \qquad (\boldsymbol{x} \in U) \tag{42}$$

is called a *k-th order system of PDEs*, where $\boldsymbol{F}: \mathbb{R}^{n^k} \times \mathbb{R}^{n^{k-1}} \times ... \mathbb{R}^n \times \mathbb{R} \times U \to \mathbb{R}^m$ given and $\boldsymbol{u}: U \to \mathbb{R}^m, \boldsymbol{u} = (u_1, ..., u_m)$ are unknowns.
The number of unknowns here is m, hence, there are m number of scalar PDEs. In cases of more unknowns than the number of equations, a set of several relations are required to solve the PDEs which are called *constitutive laws* [36].

Definition 4. A problem with a PDE model is said to be *locally well-posed* if the PDE satisfies the following [35–37]:

I The existence of a solution.

II The uniqueness of the solution.

III The solution depends continuously on the given data.

If a problem is said to satisfy Definition 4, then the problem has a solution which is very good for modeling applications such as the Ground Motion Prediction. If the problem does not satisfy all these three conditions, then the problem is called *ill-posed* and this calls for remodeling it.

There are two types of data that ensures the uniqueness of the solution of (41) or (42), and these are *initial conditions* and *boundary conditions* [36]. The

initial conditions are data usually needed for time-dependent problems which gives the value of the unknown function and/or derivative values at an initial time, say $t=0$, and is given by:

$$\nu(x,0)=g(x) \qquad \dot{\nu}(x,0)=h(x)$$

On the other hand, the boundary conditions are data that is available regarding the functional values and/or derivative values at some points along the boundary of the domain, usually at the endpoints of a line domain of length L_p, or corners of a plane, etc.

Definition 5. Given a PDE either in (41) or (42). The boundary condition is said to be of the *Dirichlet type*, if the functional values along the boundary are given in the problem, such as

$$\nu(0,t)=f_1(t) \qquad \nu\left(L_p,t\right)=f_2(t)$$

The boundary condition is said to be of the *Neumann* type, if the values of the derivative of the unknown function along the boundary are given, such as

$$\nu_x(0,t)=f_1(t) \qquad \nu_x\left(L_p,t\right)=f_2(t)$$

It is possible for the two types of boundary conditions to be used depending on the type of the data present, this is a *mixed type*, and is given by

$$\nu(0,t)=f_1(t) \qquad \nu_x\left(L_p,t\right)=f_2(t)$$

There is another type of a boundary condition called the *Robin* condition, but it is never used for an elastodynamic equation. For time-dependent problems, it is required for the PDE to have initial and boundary conditions to be classified as a well-posed. This kind of a problem is called an *initial-boundary value problem* [37].

3.1.2. **Second Order Partial Differential Equations**

The discussion of this Subsection is obtained from Zachmanoglou and Thoe [37] for the classification of second order PDEs. Let $x,y\in V$, where $V\subset \mathbb{R}$ is open. The unknown function is $u: V\times V\to \mathbb{R}$. The general form of linear second order, one-dimensional PDE in two independent variables is given by:

$$au_{xx}+2bu_{xy}+cu_{yy}+du_x+eu_y+fu+g=0 \tag{43}$$

where a,b,c,d,e,f and g are functions of both x and y. For the purpose of considering the Elastodynamic Equation with the Hooke's Law, let the functions a,b, and c be constants (or can be of class C^2 in general). It is desirable to discuss (43) in the domain $V\subset \mathbb{R}^2$ the *discriminant*

$$\Delta=b^2-ac \tag{44}$$

to classify (43) according to its sign in V. The principal part of (43) are those terms involving the second derivatives, and we wish to simplify these terms by introducing a new set of coordinates ξ and η, both are functions of $x,y\in V$. Given the initial data (x_0,y_0), there is a neighborhood $U\subset V$ of (x_0,y_0) for which (44)

can be transformed using new coordinates, and this equation is called a *canonical form* in U. Let ξ and η be expressed as the following:

$$\xi = \xi(x,y) \qquad \eta = \eta(x,y) \tag{45}$$

Let these functions be of class C^2 and have smooth non-singular transformations, and the Jacobian is not zero,

$$J \equiv \frac{\partial(\xi,\eta)}{\partial(x,y)} \equiv \xi_x\eta_y - \xi_y\eta_x \neq 0 \tag{46}$$

In a neighborhood of any point (x_0,y_0), in V where (46) is satisfied, x and t can also be expressed as functions of ξ and η (inverse):

$$x = x(\xi,\eta) \qquad y = y(\xi,\eta) \tag{47}$$

Using the chain rule, one can obtain

$$u_x = u_\xi\xi_x + u_\eta\eta_x \qquad u_y = u_\xi\xi_y + u_\eta\eta_y \tag{48}$$

and

$$\begin{aligned} u_{xx} &= u_{\xi\xi}\xi_x^2 + 2u_{\xi\eta}\xi_x\eta_x + u_{\eta\eta}\eta_x^2 + \ldots \\ u_{xx} &= u_{\xi\xi}\xi_x\xi_y + u_{\xi\eta}\xi_x\eta_y + u_{\xi\eta}\xi_y\eta_x + u_{\eta\eta}\eta_x\eta_y + \ldots \\ u_{yy} &= u_{\xi\xi}\xi_y^2 + 2u_{\xi\eta}\xi_y\eta_y + u_{\eta\eta}\eta_y^2 + \ldots \end{aligned} \tag{49}$$

Lower derivatives from (43) are expressed in the ellipses in (49) since only expressions of the principal parts matter for this discussion. Substituting (47) – (49) to (43) yields:

$$Au_{\xi\xi} + Bu_{\xi\eta} + Cu_{\eta\eta} + \ldots = 0 \tag{50}$$

where

$$\begin{aligned} A &= a\xi_x^2 + 2b\xi_x\eta_x + c\eta_x^2 + \ldots \\ B &= a\xi_x\xi_y + b\xi_x\eta_y + b\xi_y\eta_x + c\eta_x\eta_y + \ldots \\ C &= a\xi_y^2 + 2b\xi_y\eta_y + c\eta_y^2 + \ldots \end{aligned} \tag{51}$$

It can be observed that forming the expression

$$B^2 - AC = \left(b^2 - ac\right)\left(\xi_x\eta_y - \xi_y\eta_x\right)^2 \tag{52}$$

where $\Delta' = \Delta J^2$ is the modified discriminant in the variables ξ and η. If this transformation of coordinates is smooth and non-singular, then the sign of the discriminant in (44) does not change. Hence, a theorem is proven as a consequence of this.

Theorem 1. Under a smooth nonsingular transformation of coordinates, the sign of the discriminant (44) in the PDE in (43) with two independent variables does not change.

Hence, the discriminant of (43) is an inherent property which is independent of any coordinate system to be used. The value of this discriminant can be positive, zero, or negative, which renders three types of a second order linear PDE.

Definition 6. Let from (44) be the discriminant for (43). Then, if:

a $\Delta > 0$ at at the point (x_0, y_0), then (43) is a *hyperbolic* PDE at (x_0, y_0)

b $\Delta = 0$ at at the point (x_0, y_0), then (43) is a *parabolic* PDE at (x_0, y_0)

c $\Delta < 0$ at at the point (x_0, y_0), then (43) is a *elliptic* PDE at (x_0, y_0)

3.2. Elastodynamic Equation with Hooke's Law

Now, in light of the discussion in Subsection 3.1, the system of linear PDEs which is given by (40) from Section 2:

$$\begin{cases} \rho \frac{\partial \nu}{\partial t} = \frac{\partial \tau}{\partial x} \\ \\ \frac{\partial \tau}{\partial t} = \mu \frac{\partial \nu}{\partial x} \end{cases} \tag{40}$$

will be discussed here in this Subsection. It is worth noting that the density ρ and the shear modulus μ are assumed to be constants, $x \in \left[0, L_p\right], t \in [0, T]$, and both $|\nu| \leq \nu_{max}$, $\tau \leq \tau_{max}$ are bounded, with L_p being the length of the wave propagation, or the distance of the source to the site, and T being the duration of the seismogram. By adding the time derivative in the first equation to the space derivative in the second equation from (39), one can obtain

$$\frac{\partial^2 \nu}{\partial t^2} = \beta^2 \frac{\partial^2 \nu}{\partial x^2} \tag{53}$$

which is a homogenous, linear second order PDE also known as the *elastic wave* equation with $\beta = \sqrt{\mu/\rho}$ also known as the S-wave velocity [17, 32]. This is also the propagation speed of an S-wave across the material of the earth, which causes the shearing action. Since this is only in one-dimension, this only involves the SH component of an S-wave which is enough for the purpose of finding the PGA on a given site.

To show that (40) is hyperbolic, the value of the discriminant can be obtained with $A = 1$, $B = 0$ and $C = -\beta^2$ using (44):

$$\Delta = 0^2 - (1)\left(-\beta^2\right) = \beta^2 > 0$$

Wave equations in the form of $u_{tt} - c^2 u_{xx} = 0$ are hyperbolic equations which can be used as models for describing the vibration of a string (in 1D), a membrane (in 2D), or an elastic solid (in 3D) [35, 36], and acoustic waves on a pipe [37, 32]. Another way to show that (40)is hyperbolic is by writing it in a compact form:

$$\boldsymbol{w}_t + \boldsymbol{A}(x,t)\boldsymbol{w}_x = \boldsymbol{0} \tag{54}$$

where

$$\boldsymbol{w} = \begin{pmatrix} v \\ \tau \end{pmatrix} \qquad \boldsymbol{A} = \begin{pmatrix} 0 & -1/\rho \\ -\mu & 0 \end{pmatrix}$$

Definition 7 [36, 37]. If matrix $\boldsymbol{A}$ in the system in (54) has real and distinct eigenvalues, then(54) is said to be a hyperbolic system in a domain, say $\left(0, L_p\right) \times (0, T)$ for this problem.

The characteristic equation of matrix $\boldsymbol{A}$ is $\lambda^2 - \mu/\rho = 0$ with roots $\lambda = \pm\sqrt{\mu/\rho} = \pm\beta$ which are the eigenvalues that are real and distinct. Hence, (40) is of a

hyperbolic type. According to Li and Chen [38], (54) is well-posed given the appropriate initial and boundary conditions, if matrix $\boldsymbol{A}$ has real eigenvalues and each eigenvalue has a corresponding eigenvector.

3.2.1. **Initial and Boundary Conditions**

Since (39) was used in predicting the ground motion, the initial and boundary conditions on velocity and stress were required to solve the problem. The following data is assumed for velocity:

$$\nu(0,t)=0 \qquad \nu(x,)=0 \tag{55}$$

which is appropriate since the velocity at $x=L_p$ is required which represents the seismogram needed for the ground motion prediction. The interpretation of zero velocity at the boundary means that the boundary is rigid, but the stress in not zero. On the other hand, it is assumed that initially, the fault is at rest and so the system is in equilibrium [33].

For the initial condition, the traction must be zero since the rocks outside the fault are in equilibrium at time $t=0$ [33]. For the boundary condition, the *time-weakening friction law* [7] was adapted which assumes that in a point source, the stress variation is due to the stress drop during an earthquake and is governed by the friction in the fault. For this study, this friction model was modified considering the time to permit the propagation of cracks during rupture. The resulting boundary condition is given by

$$\tau(0,t)=\begin{cases} \frac{1}{2}(\tau_0+\tau_1)+\frac{t}{2t_r}(\tau_0-\tau_1), & 0\le t_r\le t \\ \left[\tau_0-(\tau_0-\tau_1)\frac{t-t_r}{t_1}\right], & t_r<t\le t_1 \\ \tau_1, & t>t_1 \end{cases} \tag{56}$$

where τ_0 and τ_1 are the static and dynamic stresses in the fault, t_r is the rupture time (or the rise time) which is the total time of propagation of cracks in the fault zone of length L approximately equal to $0.5L/\nu_r$ for bilateral rupture [39] and $\nu_r=0.9\beta$ is the rupture velocity which is an assumed value [32], t_1 is the time that it takes to decrease the shear stress from τ_0 to τ_1. The value of t_r can be viewed also as the time it takes for the stress to rise from a certain value of stress, say $1/2(\tau_0+\tau_1)$ to τ_0, which assumes that the point source is stressed initially before the fault moves and releases the energy during the earthquake. This model assumes that under no earthquake occurrences, the shear stress acting in the fault is the dynamic shear stress. The profile of stress at all values of time $t\ge 0$ is shown in Figure 16.

According to Bizzarri [7], the shaded area in Figure 16 is the fracture energy G while the change from static stress to dynamic stress is what is referred to as the stress drop $\Delta\sigma$ [32], which can be estimated by the formulation obtained from (10) by Causse, Dalguer, and Mai [31]. To apply the modified friction law for this study, τ_1 is assumed to be zero which implies that the fault will be completely relieved of

the shear stress upon the release of seismic waves. Therefore, the modified friction law for the boundary condition at the source implies that upon rupture of the fault, there is an increase in stress at that point from $\tau_0/2$ to $\tau_0 = \Delta\sigma_d$ (stress drop) with duration of t_r, then decreasing the linearly from τ_0 to zero, and no residual stresses will be left in the fault.

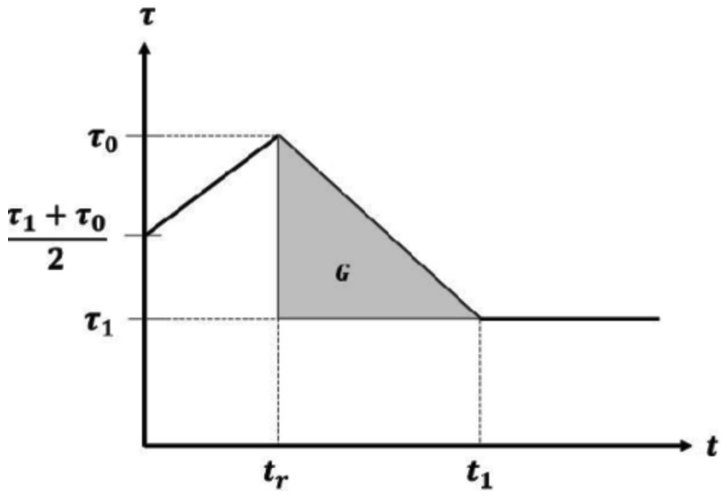

Figure 16. Modified time-weakening friction law

3.3. Numerical Solution to Partial Differential Equations

There are many ways to solve PDEs and each of them has its own pros and cons. Analytical (explicit) solutions can be obtained by representation formulas, transform methods, or separation of variables. Numerical solutions can be utilized such as the finite difference method, the finite element method, or meshless methods, which offer approximations to the exact solutions depending on the complexity of the PDE for which viable exact solutions cannot be obtained. is is only the finite difference method will be discussed in this paper, while other types of finding a solution are not within the scope of this study.

3.3.1. Finite Difference Approximations to Elastodynamic Equation and Hooke's Law

In the finite difference method, the function and its derivatives are approximated using the Taylor expansion. The Taylor expansion for $\nu(x+h)$ for a small increment h is given by:

$$\nu(x+h) = \nu(x) + h\,\nu'(x) + \frac{h^2}{2}\nu''(x) + \frac{h^3}{6}\nu'''(x) + O(h^3) \tag{57}$$

Similarly, $\nu(x+h)$ is obtained in the same fashion:

$$\nu(x-h) = \nu(x) - h\,\nu'(x) + \frac{h^2}{2}\nu''(x) - \frac{h^3}{6}\nu'''(x) + O(h^3) \tag{58}$$

Using (58) and (59), the derivates of the function can be approximated. For the elastodynamic equation and the Hooke's Law, it is the first derivatives only that appear, and hence, these are the only derivatives considered in this study. The first derivative can be expressed using *forward differencing, backward differencing*, and *central differencing*. Using forward differencing, the first derivative of $\nu(x)$ can be approximated as:

$$\nu'(x) = \frac{\nu(x+h)-\nu(x)}{2h} + O(h) \tag{59}$$

with a very small step size h. Using backward differencing, the expression for the derivative is given by:

$$\nu'(x) = \frac{\nu(x)-\nu(x-h)}{2h} + O(h) \tag{60}$$

Using the central differencing, the derivative can be approximated as:

$$\nu'(x) = \frac{\nu(x+h)-\nu(x-h)}{2h} + O(h^2) \tag{61}$$

which has a double step size. While the first two expressions of the first derivative are first-order accurate, the last one is a second-order accurate. Virieux [33] used central differencing to approximate the spatial derivative, with the same step size, but on a staggered-grid, which results in a more accurate approximation up to four times smaller than a normal grid. Figure 17 shows how stress and velocity grids are formulated by Virieux [33]. Using the approach used by Virieux, the first derivative is given by:

$$\nu'(x) = \frac{\nu(x+h/2)-\nu(x-h/2)}{h} + O(h^2) \tag{62}$$

For simplicity in differencing in space, $\nu(x+h)$ is denoted by ν_{j+1}, while $\nu(x-h)$ is denoted by ν_{j-1}; for differencing in time, $\nu(t+k)$ is denoted by ν^{i+1} while $\nu(t-k)$ is denoted by ν^{i-1}.

Now, let the problem involving the ground motion prediction be recalled and given by (63):

$$\begin{cases} \rho\frac{\partial \nu}{\partial t} - \frac{\partial \tau}{\partial x} = 0 & \\ & (x,t) \in \left[0, L_p\right] \times [0,T] \\ \frac{\partial \tau}{\partial t} - \mu\frac{\partial \nu}{\partial x} = 0 & \\ \nu(x,0) = 0 \qquad \tau(x,0) = 0 & x \in \left[0, L_p\right] \\ \nu(0,t) = 0 \qquad \tau(0,t) = f(t) & t \in [0,T] \end{cases} \tag{63}$$

where $f(t)$ is given by (56).

Let the grid spacing Δx be chosen arbitrarily and let it be set equal to L_p/J, where J is the number of grid points, and the time step Δt be any very small number for a moment (this will be discussed later in Subsection 3.3.2). Let the

interior of the computation domain $\left[\boldsymbol{0}, \boldsymbol{L_p}\right] \times [\boldsymbol{0}, \boldsymbol{T}] \in \left(\boldsymbol{x_j}, \boldsymbol{t^i}\right)$ be discretized in the following manner:

$$\begin{aligned} x_j &= x_{j-1} + j\Delta x \qquad 1 \le j \le J \\ t^i &= t^{i-1} + i\Delta t \qquad 1 \le i \le 1 \end{aligned} \tag{64}$$

Using (61) and (62), (63) can be approximated as [33, 40, 32]:

$$\begin{cases} \nu_j^{i+1/2} = \nu_j^{i-1/2} + \frac{\Delta t}{\Delta x} \frac{\tau^i_{j+1/2} - \tau^i_{j-1/2}}{\rho} & 1 \le i \le I,\ 1 \le j \le J \\ \tau^{i+1}_{j+1/2} = \tau^i_{j+1/2} + \mu \frac{\Delta t}{\Delta x} \left[\nu^{i+1/2}_{j+1} - \nu^{i+1/2}_j\right] & (x,t) \in \left(0, L_p\right) \in (0,T) \end{cases} \tag{65}$$

where the subscripts indicate differencing in space and the superscripts indicate differencing in time. In this approach, velocities and stresses are stored in different points, with a step offset of half in space and time. It is implicit to the numerical scheme in (65) that the initial conditions required for this problem are obtained at $t = -\Delta t/2$ and at $t = \Delta t/2$. Similarly, the boundary conditions are obtained at $x = -\Delta x/2, \Delta x/2$. The central differencing in time is similar with (61), while that in space is shown in (62), hence, the staggered grid approach. The velocity and the pressure are still obtained from the same grid points, but the values required from the approximation are half-steps to the left and to the right, and up and down of the grid point, just like a five-point stencil. As mentioned by Shearer [32], the error in the approximation is four time smaller since the sampling is halved. For the pressure at the boundary, it is assumed that it is the same in the vicinity of the fault rupture point within the half of the grid spacing to the left and right, and zero outside the vicinity of the point.

3.3.2. Consistency, Stability, and Convergence of Finite Difference Approximations

For the purpose of discussion of the properties of the numerical scheme in (65), some definitions from Li and Chen [38] were used here to ensure a unique solution for given initial and boundary data.

Definition 8. The *truncation errors* of the scheme in (65) are defined as

$$TE_1(x,t) = \frac{\nu(x,t+\Delta t/2) - \nu(x,t-\Delta t/2)}{\Delta t} - \frac{1}{\rho} \frac{\tau(x+\Delta x/2,t) - \tau(x-\Delta x/2,t)}{\Delta x}$$

$$TE_2(x,t) = \frac{\tau(x,y+\Delta t/2) - \tau(x,t-\Delta t/2,)}{\Delta t} - \mu \frac{\nu(x+\Delta x/2,t) - \nu(x-\Delta x/2,t)}{\Delta x} \tag{66}$$

Definition 9. The scheme in (65) is said to be consistent with the differential equations in (40), if the truncation errors in (66) approach zero as $\Delta x,\ \Delta t \to 0$ for any $(x,t) \in \left(\Delta x/2, L_p\right) \times (\Delta t/2, T)$.

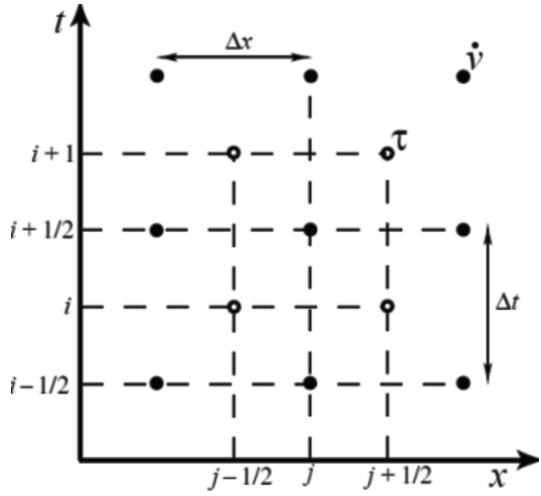

Figure 17. A staggered grid in which velocities and stresses are stored at different points. *Source: Shearer, 2009 [32]*

Definition 10. The scheme in (65) is said to be *stable* under the norm $||\cdot||$ for a time-dependent PDE if there exists a constant M such that

$$\left||u^i|\right| \leq M\left||u_i^0|\right| \qquad \forall i \;\; \Delta t, \leq T \tag{67}$$

where M is independent of $\Delta x, \Delta t$ and the initial condition u^0.

Definition 11. Let the exact and numerical solutions to (40) and (65) be denoted by $U_{PDE}(x,t)$ and $u_{FD}(x_j,t^i)$. The scheme in (67) is said to convergent if

$$|u_{PDE} - u_{FD}| \to 0 \qquad \Delta x, \Delta t \to 0 \tag{68}$$

Theorem 2 (Lax-Richtmyer). For the scheme formulated in (65) to be a well-posed linear time-dependent problem, (65) must be both consistent and stable for the convergence of the solution.

Clearly, using the above definition, (65) is consistent with (40) as Δx, $\Delta t \to 0$, for any $(x,t) \in \left(0, L_p\right) \in (0,T)$. To prove that (65) is stable, the von Neumann Stability analysis will be invoked, which is used for the linear constant coefficient problem [38]. If the formulation in (65) is both consistent and stable, then Theorem 2 can be invoked to claim that (40) has a unique solution numerically which depends on the given initial and boundary data.

To use the von Neumann Stability Analysis [40], the solution to (65) is assumed to be in the form of exponential functions just like what is done in separation of variables, and then obtaining a Fourier Series for the superposition of solutions. Assume that ν and τ in the form

$$\begin{aligned} \nu_j^n &= A \exp(-i\omega n\, \Delta t + ikj\, \Delta x) \\ \tau_j^n &= B \exp(-i\omega n\, \Delta t + ikj\, \Delta x) \end{aligned} \tag{69}$$

where ν_j^n, τ_j^n are velocity and traction at $x = x_j$ and $t = t^n$ (to avoid confusion with the use of index i and imaginary unit $i = \sqrt{-1}$, n is used for showing stability), A, B are constants (or amplitude of the wave), ω, k are the wave numbers of the solution. Substituting (68) to the velocity and traction terms in the right-hand sides of the equations, one obtains:

$$\begin{aligned}
&\nu_{j+1}^{n+1/2} - \nu_j^{n+1/2} = \\
&\quad = \mathrm{A}\exp\left(-i\omega(n+1/2)\Delta t + ik(j+1)\Delta x\right) - A\exp\left(-i\omega(n+1/2)\Delta t + ikj\Delta x\right) \\
&\quad = \mathrm{A}\exp\left(-i\omega(n+1/2)(\Delta t) + ikj\,\Delta x/2\right)\left[\exp\left(ik\,\Delta x/2\right) - \exp\left(-ik\Delta x/2\right)\right] \\
&\quad = \nu_{j+1/2}^{n+1/2}\left[2\,i\sin\tfrac{k\Delta x}{2}\right] \\
&\tau_{j+1/2}^{n} - \tau_{j-1/2}^{n} = \\
&\quad = \mathrm{B}\exp\left(-i\omega n\,\Delta t + ik(j+1/2)\,\Delta x\right) - B\exp\left(-i\omega n\,\Delta t + ik(j-1/2)\,\Delta x\right) \\
&\quad = \mathrm{B}\exp\left(-i\omega n\,\Delta t + ik(j+1/2)\,\Delta x\right)\left[\exp\left(ik\,\Delta x/2\right) - \exp\left(-ik\Delta x/2\right)\right] \\
&\quad = \tau_j^n\left[2\,i\sin\tfrac{k\Delta x}{2}\right]
\end{aligned} \tag{70}$$

Substituting the final expressions of the velocity and traction terms in (65), the scheme becomes

$$\begin{aligned}
\nu_j^{n+1/2} &= \nu_j^{n-1/2} + \frac{1}{\rho}\frac{\Delta t}{\Delta x}\tau_j^n\left[2\,i\sin\frac{k\Delta x}{2}\right] \\
\tau_{j+1/2}^{n+1} &= \tau_{j+1/2}^{n} + \mu\frac{\Delta t}{\Delta x}\nu_{j+\frac{1}{2}}^{n+\frac{1}{2}}\left[2\,i\sin\frac{k\Delta x}{2}\right]
\end{aligned} \tag{71}$$

Adjusting the second equation of (71) to be in the same grid point as that of the first equation, one obtains:

$$\tau_j^{n+1/2} = \tau_j^{n+1/2} + \mu\frac{\Delta t}{\Delta x}\nu_j^n\left[2i\sin\frac{k\Delta x}{2}\right] \tag{72}$$

Let $\Delta = \Delta t/\Delta x$ and $\hat{S}\sin(k\Delta x/2)$. The scheme in (71) with (69) can be rewritten as

$$\begin{cases}
\nu_j^{n+1/2} = \nu_j^{n-1/2} + \frac{2i}{\rho}\hat{S}\Delta\tau_j^n \\
\qquad \nu_j^n = \nu_j^n \\
\tau_j^{n+1/2} = \tau_j^{n-1/2} + 2i\mu\hat{S}\Delta\nu_j^n \\
\qquad \tau_j^n = \tau_j^n
\end{cases} \tag{73}$$

which can be expressed in a matrix form

$$\boldsymbol{U_j^{n+1/2}} = \boldsymbol{G}\,\boldsymbol{U_j^n} \tag{74}$$

where

$$\boldsymbol{U_j^{n+1/2}} = \begin{bmatrix} \nu_j^{n+1/2} \\ \nu_j^n \\ \tau_j^{n+1/2} \\ \tau_j^n \end{bmatrix} \quad \boldsymbol{G} \begin{bmatrix} 0 & 1 & \frac{2i}{\rho\hat{S}\Delta} & 0 \\ 1 & 0 & 0 & 0 \\ 2i\mu\hat{S}\Delta & 0 & 0 & 1 \\ 0 & 0 & 1 & 0 \end{bmatrix} \quad \boldsymbol{U_j^n} = \begin{bmatrix} \nu_j^n \\ \nu_j^{n-1/2} \\ \tau_j^n \\ \tau_j^{n+1/2} \end{bmatrix}$$

The matrix G is called the *amplification factor*, which does not depend on time since it is obtained from the constant coefficients of the terms of the linear PDE [40]. Hence, one can write (74) into

$$\boldsymbol{U_j^{n+1/2}} = \boldsymbol{G^{m+1}}\,\boldsymbol{U_j^0} \tag{75}$$

since $\boldsymbol{G}$ does not depend on time and $\left\|\boldsymbol{U_j^n}\right\| \leq \left\|\boldsymbol{U_j^0}\right\|$ from (69), and since

$$\left\|\boldsymbol{U_j^{n+1/2}}\right\| = \left\|\boldsymbol{G^{m+1}}\,\boldsymbol{U_j^n}\right\| \leq \|\,\boldsymbol{G}\,\|^{m+1}\left\|\boldsymbol{U_j^0}\right\|$$

the numerical solution will be bounded if and only if

$$\|\,\boldsymbol{G}\,\| \leq 1 \tag{76}$$

where $\|\cdot\|$ is a matrix norm. It is sufficient for the condition in (75) for the stability of the numerical scheme in (65). It is required for the maximum of the eigenvalues of $\boldsymbol{G}$ to have the modulus less than or equal to unity to satisfy the von Neumann stability.

The characteristic equation for matrix $\boldsymbol{G}$ in (74) is

$$1 - 2\lambda^2 + 4\Delta^2\hat{S}^2\frac{\mu}{\rho}\lambda^2 + \lambda^4 = 0 \tag{77}$$

It is then required that the roots of (77) have absolute values smaller than or equal to one. Letting $z = \lambda^2$ and $a = \Delta^2\hat{S}^2\mu/\rho$, the equation in (77) becomes

$$z^2 + (4a - 2)z + 1 = 0$$

the roots of which are

$$z_{1,2} = -2a + 1 \pm 2\sqrt{a^2 - a} \tag{78}$$

If $0 < a \leq 1$, then $|z_{1,2}| \leq 1$ which is the stability condition. Then, it follows that

$$\Delta^2\frac{\mu}{\rho}\hat{S}^2 = \left(\frac{\Delta t}{\Delta x}\right)^2\frac{\mu}{\rho}\sin^2\left(\frac{k\Delta x}{2}\right) \leq 1 \tag{79}$$

Hence, the condition for the time and space increments for the staggered grid is obtained so that the numerical scheme in (65) is stable, and this condition is given by

$$\Delta t \leq \Delta x\left(\frac{\rho}{\mu}\right)^{1/2} = \frac{\Delta x}{\beta} \tag{80}$$

where β is the speed of the S-wave propagation from (53). Hence, the scheme in (65) is *conditionally stable*.

Since (65) is consistent and stable given that (79) is satisfied, t hen by the Lax-Richtmyer Theorem, the numerical solution to (65) is convergent. The condition in (79) or (80) is called the *Courant-Friedrich-Levy* (CFL) condition [38]. To ensure stability, the time step must be a fraction of the ratio of the grid spacing and the S-wave velocity. This fraction is called the CFL number, which is equal to $\beta\Delta t/\Delta x$.

The required preliminary concepts for the ground motion prediction and how to solve it numerically have been presented so far. The next Section will discuss in detail the PSHA Methodology to estimate the feasible ground shaking level on a site with relaxation of the ergodic assumption of the Classical PSHA.

REFERENCES

[1] Kramer S L 1996 *Geotechnical earthquake engineering*, Prentice-Hall Inc, New Jersey 1

[2] Kramer S L and Scawthorn C 2000 *Geotechnical earthquake considerations*, *Bridge Engineering Handbook*, Wai-Fah Chen and Lian Duan. Boca Raton: CRC Press, **132**

[3] Monaco P, Totani G, Barla G, Cavallaro A, Costanzo A, D'Onofrio A, Evangelista L, Foti S, Grasso S, Lanzo G, Madiai C, Maraschini M, Marchetti S, Maugeri M, Pagliaroli A, Pallara O, Penna A, Saccenti A, De, Magistris F S, Scasserra S, Silvestri F, Simonelli A L, Simoni G, Tommasi P, Vannucchi G, and Verrucci L 2009 *Geotechnical aspects of the L'Aquila Earthquake*, *Earthquake Geotechnical Engineering Satellite Conference XVIIth International Conference on Soil Mechanics & Geotechnical Engineering, Alexandria, Egypt*

[4] Papanikolaou I D, Lekkas E L, Roberts G P, McGuire B, Fountoulis I G, Parcharidis I, and Foumelis M 2010 *The 2009 L'Aquila earthquake; findings and implications Event Science Report 02, AON Benfield UCL Hazard Research Centre*, *Event Science Report 02*, AON Benfield UCL Hazard Research Centre

[5] Coburn A and Spence R 2002 *Earthquake protection 2nd Edition*, John Wiley & Sons, Ltd., England 73

[6] Hutchings, L and Viegas G 2012 *Application of Empirical Green's Functions in earthquake source, wave propagation and strong ground motion studies*, *Earthquake Research and Analysis - New Frontiers in Seismology Sebastiano D'Amico (Ed)*

[7] Bizzarri A 2011 *On the deterministic description of earthquakes*, *Reviews of Geophysics* **49** 1

[8] Paolucci R, Infantino M, Mazzieri I, Özcebe A G, Smerzini C, and Stupazzini M 2017 *3D physics-based numerical simulations: advantages and current limitations of a new frontier to earthquake ground motion prediction The Istanbul case study*, *MOX Technical Report 68/2017*, Dipartimento di Matematica Politecnico di Milano, Via Bonardi 9 - 20133 Milano Italy

[9] McGuire R K 2001 *Deterministic vs probabilistic earthquake hazard and risks*, *Soil Dynamics & Earthquake Engineering* **21** 377
[10] Cornell C A 1968 *Engineering seismic risk analysis*, *Bulletin of the Seismological Society of America* **58** 1583
[11] McGuire R K 2007 *Probabilistic seismic hazard analysis: Early history*, *Earthquake Engineering and Structural Dynamics* **37** 329
[12] Anderson J G and Brune J N 1999 *Probabilistic seismic hazard analysis without the ergodic assumption*, *Seismological Research Letters* **70** 19
[13] Landwehr N, Kuehn N M, Scheffer T and Abrahamson N 2016 *A Non-Ergodic Ground-Motion Model for California with Spatially Varying Coefficients*, *Bulletin of the Seismological Society of America* **106** (6) 2574
[14] Bazurro P and Cornell A C 1999 *Disaggregation of seismic hazard*, *Bulletin of Seismological Society of America* **89** 501
[15] McGuire R K 1995 *Probabilistic seismic hazard analysis and design earthquakes: closing the loop*, *Bulletin of the Seismological Society of America* **85** 1275
[16] Kotha S R, Bindi D and Cotton F 2017 *Towards a non-ergodic probabilistic seismic hazard assessment In Europe and Middle East*, *16th World Conference on Earthquake, 16WCEE 2017: Santiago, Chile*
[17] Aki K. and Richards P G 2002 *Quantitative Seismology (2nd Edition)*, University Science Books, Sausalito, California, U.S.A.
[18] Hutchings L, Ioannidou E, Foxall W, Voulgaris N, Savy J, Kalogeras I, Scognamiglio L, and Stavrakakis G 2007 *A physically based strong ground-motion prediction methodology; application to PSHA and the 1999 Mw = 6.0 Athens earthquake*, *Geophysics Journal International* **168** 659
[19] Tarbali K, Bradley B, Huang J, Polak V, Lagrava D, Motha J, and Bae S 2018 *CYBERSHAKE NZ V179: New Zealand simulation-based probabilistic seismic hazard analysis*, *16th European Conference on Earthquake Thessaloniki Engineering*
[20] Tarbali K, Bradley B, Huang J, Lee R, Lagrava D, Bae S, Polack V, Motha J, and Zhu M 2019 *CYBERSHAKE NZ V185: New Zealand simulation-based probabilistic seismic hazard analysis*, *2019 Pacific Conference on Earthquake Engineering - New Zealand Society for Earthquake Engineering*
[21] Field E H, Jordan T H and Cornell C A 2003 *OpenSHA: a developing community modeling environment for seismic hazard analysis*, *Seism. Res. Lett.* **74** (4) 406
[22] Solomos G, Pinto A, and Dimova S 2008 *A Review of The Seismic Hazard Zonation in National Building Codes in the Context of Eurocode 8*, *European Commission, Varese Italy*, Joint Research Center JRC Technical Report
[23] Wald D J V, Quitoriano, Heaton T H, and Kanamori H 1999 *Relationships between peak ground acceleration, peak ground velocity and modified Mercalli intensity in California*, *Earthquake Spectra* **15** 557
[24] Valentini A, Pace B, Boncio P, Visini F, Pagliaroli A, and Pergalani F 2019 *Definition of seismic input from fault-based PSHA: Remarks after the 2016 Central Italy earthquake sequence*, *AGU 100: Advancing Earth and Space Science*
[25] Valentini A, Visini F, and Pace B 2017 *Integrating faults and past earthquakes into a probabilistic seismic hazard model for peninsular Italy*, *Natural Hazards and Earth System Sciences* **17** (11) 2017
[26] Molas G L, Yamazaki F, and Tomatsu Y 1994 *Seismic hazard analysis in the Philippines using earthquake recurrence data*, *Earthquake Engineering*, Tenth World Conference Balkema, Rotterdam 6031
[27] McGuire R K *Computations of seismic hazard*, *Annali di Geofisica* **36** 181
[28] Scordilis E M 2006 *Empirical global relations converting M_s and m_b to moment magnitude*, *Journal of Seismology* **10** 225

[29] Kanamori H 1977 *The energy release in great earthquakes*, *Journal of Geophysical Research* **82** 2981

[30] Hanks T C and Kanamori H 1979 *A moment magnitude scale*, *Journal of Geophysics Research* **84** 2348

[31] Causse M, Dalguer L A and Mai P M 2013 *Variability of dynamic source parameters inferred from kinematic models of past earthquakes*, *Geophysical Journal International* **196** (3) 607

[32] Shearer P 2009 *Introduction to Seismology 2nd ed*, *Cambridge University Press, New York*

[33] Virieux J 1984 *SH-wave propagation in heterogeneous media: Velocity-stress finite-diffe-rence method*, *Geophysics* **49** (11) 1933

[34] Schuster G T 2017 *Seismic Inversion*, Society of Exploration Geophysicists 166

[35] Evans L C 1997 *Partial Differential Equations. Graduate Studies in Mathematics Vol. 19*, American Mathematical Society

[36] Salsa S 2008 *Springer-Verlag, Italy, Milano*, Partial differential equations in action: From modelling to theory

[37] Zachmanoglou E C, and Thoe D W 1986 *Introduction to Partial Differential Equations with Applications*, *Dover Publications, Inc, New York*

[38] Li J and Chen Y T 2008 *Computational Partial Differential Equations Using MATLAB*, CRC Press, Taylor & Francis Group, Boca Raton

[39] Kanamori H and Brodsky E M 2004 *The physics of earthquakes*, *Rep. Prog. Phys* **67** 1429

[40] Mozco P, Kristek J, and Halada L 2004 *The finite-difference method for seismologists -An introduction*, *Comenius University, Bratislava*